Specialisation of meiotic kinetochores revealed through a synthetic SAC strategy

Lori B Koch[1], Christos Spanos[1,2], and Adele L Marston[1,2]*

* Correspondence to: adele.marston@ed.ac.uk

[1]Centre for Cell Biology, School of Biological Sciences, University of Edinburgh, Edinburgh EH9 3BF, UK.
[2]Discovery Research Platform for Hidden Cell Biology, School of Biological Sciences, University of Edinburgh, Edinburgh EH9 3BF, UK.

Abstract

Meiosis creates haploid gametes through two sequential M phases. While many studies have focused on meiosis I, the molecular events which drive and define meiosis II are largely unknown. Here, we report a novel cell synchronization strategy which allows for collection of yeast cells arrested at metaphase I or metaphase II, enabling better characterisation of meiosis II events. The method relies on chemically-inducible dimerization of ectopic copies of spindle assembly checkpoint (SAC) proteins Mps1 and Spc105. Using this synthetic SAC (SynSAC) approach, we found that the SAC response is weaker in metaphase I compared to metaphase II and that the PP1 binding site within Spc105 contributes to restraining the MI SAC response. Furthermore, we demonstrate the utility of the SynSAC approach by analysing the composition and phosphorylation of kinetochores from metaphase I and metaphase II. This revealed an increase in the abundance of outer kinetochore proteins in meiotic metaphase I and reduced phosphorylation on metaphase II kinetochore proteins. Overall, we present the SynSAC method as a valuable tool for analysis of both meiotic metaphases.

Introduction

To make haploid gametes for sexual reproduction, diploid cells undergo meiosis which consists of a single round of DNA replication followed by two sequential chromosome segregation events, meiosis I and meiosis II. In meiosis I, maternal and paternal chromosomes, called homologs, separate, while in meiosis II, sister chromatids separate, similar to mitosis. To achieve this, the sister chromatids within each homolog are mono-oriented toward the same spindle pole in meiosis I but bi-oriented towards opposite poles in meiosis II. This requires that kinetochores, large protein complexes which connect chromosomes to spindle microtubules, must establish mono-orientation in meiosis I and then convert to bi-orientation in meiosis II. The sequential segregation of homologs and sister chromatids further rely on the step-wise loss of sister chromatid cohesion coupled to two consecutive rounds of spindle assembly and disassembly (reviewed in (Duro & Marston, 2015)). How these key cell biological events are established and coupled in meiosis to allow two distinct rounds of chromosome segregation without an intervening S phase is not well understood. In human oocytes, meiotic chromosome segregation is error-prone and aneuploidy is common (Gruhn & Hoffmann, 2022). Thus identifying molecular mechanisms which prevent improper chromosome segregation may help efforts to improve fertility.

A major barrier in defining molecular events that direct the two meiotic divisions is a lack of synchronization tools which allow collection of populations of cells at key meiotic stages. While mammalian oocytes naturally arrest in metaphase II, material is limited, which precludes biochemical analysis. *Xenopus* oocytes provide a powerful system for analysis of metaphase II extracts but isolation of pure metaphase I populations is challenging (Peshkin *et al*, 2025; Iwabuchi *et al*, 2000). Furthermore, identifying chromosome-related proteins in the comparatively large cytoplasmic volume of oocytes presents an additional impediment.

The ability to harvest large number of cells together with ease of genetic manipulation have made yeast outstanding tools for discovering the fundamental mechanisms of meiosis. However, compared to mitosis, our knowledge of meiotic chromosome segregation has lagged behind, in part due to a lack of robust synchronization systems. Nevertheless, recent advances allow reversible arrest of budding yeast at meiotic entry and prophase, allowing synchronous release into meiosis I, and subsequently meiosis II (Berchowitz *et al*, 2013; Chia & van Werven, 2016; Carlile & Amon, 2008). These systems have been used extensively, but the short time window between the divisions limits the ability to resolve pure meiosis I and II populations. Therefore, direct comparison of meiosis I and II has remained difficult to achieve in any system.

104 To overcome these challenges, we sought to establish a method that relies on
105 inducible inhibition of the Anaphase Promoting Complex (APC-Cdc20) in either meiosis I or
106 meiosis II. The APC-Cdc20 is a ubiquitin ligase that targets key substrates for degradation
107 including securin and cyclin B, which is required for progression into anaphase (Peters, 2006).
108 The requirement for the APC-Cdc20 at both meiosis I and II is well-established and placement
109 of the gene for the APC activator, *CDC20*, under control of a meiotically-repressed promoter
110 has been widely used to arrest budding yeast cells in metaphase I (Lee & Amon, 2003). This
111 system has also been adapted to allow re-expression of *CDC20* and synchronous meiosis II
112 entry (Argüello-Miranda *et al*, 2017) as well as re-expression of the *cdc20-3* temperature
113 sensitive allele to enable collection of metaphase II cells (Mengoli *et al*, 2021). However, the
114 reliance on transcriptional control and temperature shift results in a slower response than
115 desirable. Therefore, no tools currently exist to quickly and reliably enrich budding yeast cell
116 populations in meiosis II.
117 The APC-Cdc20 is a natural target of the spindle assembly checkpoint (SAC), a
118 signalling cascade that prevents anaphase when chromosomes are not properly attached to
119 the spindle (McAinsh & Kops, 2023). The SAC is initiated at improperly attached kinetochores
120 when the kinase Mps1 phosphorylates the kinetochore protein Spc105^{KNL1}. This
121 phosphorylation recruits the checkpoint proteins Bub3/Bub1 and then Mad1/Mad2 to the
122 kinetochore. Within this kinetochore complex, Mad2 is converted from the open to closed
123 conformation and C-Mad2 associates with Mad3^{BubRI}, Bub3, and Cdc20 to form the mitotic
124 checkpoint complex (MCC), a diffusible inhibitor of the anaphase promoting complex (APC).
125 Sustained SAC activation, resulting in prometaphase arrest, can be induced experimentally
126 by perturbing kinetochore-microtubule interactions, for example by treatment with
127 microtubule-depolymerizing drugs, and this method has been used extensively in mitotic cells.
128 However, meiotic cells respond poorly to such drugs, likely due to a combination of impaired
129 uptake, toxicity and a weakened checkpoint (Hochwagen *et al*, 2005; MacKenzie *et al*, 2023).
130 Moreover, such treatments are unsuitable for analysis of kinetochore function since they
131 ablate microtubule interactions and convert kinetochores into a signalling platform, thereby
132 changing their composition and properties.
133 An alternative approach to arrest cells in either metaphase I or II would induce SAC-
134 dependent APC-Cdc20 inhibition without perturbing kinetochores. Mechanistic studies in
135 fission yeast and human cells have achieved inducible activation of the SAC through
136 conditional dimerization of Mps1 kinase and Spc105^{KNL1} (Aravamudhan *et al*, 2015; Amin *et*
137 *al*, 2018; Leontiou *et al*, 2019; Chen *et al*, 2019). Here, we adapted this approach to arrest
138 cells in either metaphase I or metaphase II of meiosis. We demonstrate that induced

139 dimerization of Mps1 and Spc105^{KNL1} engineered to lack their kinetochore-targeting domains
140 efficiently arrests cells in either metaphase I or metaphase II, in addition to mitotic metaphase.
141 This synthetic SAC (SynSAC)-dependent arrest relies on the same downstream signalling
142 cascade required for APC-Cdc20 inhibition during mitotic division, culminating in stabilization
143 of the anaphase inhibitor Pds1^{securin}. We find that the SynSAC arrest is more potent in
144 metaphase II than metaphase I, and provide evidence that protein phosphatase 1 (PP1) limits
145 the duration of the SAC-mediated metaphase I delay. To demonstrate the utility of our SynSAC
146 approach, we purified kinetochores from metaphase I, metaphase II, and mitotic metaphase
147 SynSAC cells and analysed their composition and phosphorylation using mass spectrometry.
148 This provided evidence that the relative enrichment of purified core kinetochore sub-
149 complexes changes in meiotic metaphase I and II compared to mitotic metaphase, and that
150 overall kinetochore phosphorylation is reduced in metaphase II. Therefore, by developing
151 SynSAC as a meiotic interrogation tool we have generated a comprehensive dataset of
152 kinetochore composition and phosphorylation, a key resource to uncover the critical
153 specializations that direct distinct segregation events in meiosis I and II.
154
155 **Results**
156
157 ***A synthetic SAC prolongs metaphase I or metaphase II***
158 We sought to activate the SAC to arrest cells in metaphase without disrupting kinetochores.
159 Thus, we constructed a yeast strain which has an additional, ectopic copy of each of Spc105
160 and Mps1 lacking their kinetochore-binding domains and which can be inducibly dimerised.
161 To temporally separate populations of cells undergoing meiosis I vs meiosis II, this strain also
162 carried inducible *NDT80*, which allows synchronous release from prophase arrest upon
163 addition of b-estradiol (Carlile & Amon, 2008). To induce dimerization, we used the PYL and
164 ABI tags, which dimerise in the presence of the plant hormone abscisic acid (ABA) (Liang *et*
165 *al*, 2011; Miyazono *et al*, 2009). This system is particularly advantageous compared with the
166 widely used rapamycin-inducible dimerization system because it cannot affect endogenous
167 mTOR signalling, nor does it require background mutations to avoid toxicity. Spc105 lacking
168 its C-terminal kinetochore localization domain (Petrovic *et al*, 2014; Ghodgaonkar-Steger *et*
169 *al*, 2020; Roy *et al*, 2022; Maskell *et al*, 2010), and tagged with PYL, was produced from its
170 endogenous promoter (Spc105$^{(1-455)}$-PYL). Similarly, the C-terminal kinase domain of Mps1,
171 also under the control of its native promoter and lacking the N-terminal disordered domain
172 which mediates its kinetochore localization, was fused to ABI (Mps1$^{(440-765)}$-ABI) (Figure
173 1A)(Araki *et al*, 2010). As expected, spore viability of this “SynSAC” strain after prophase

174 release was comparable to that of a strain lacking the ABI/PYL tagged truncations, indicating
175 that meiosis was not impaired by these constructs (Figure 1B).
176 Following prophase release in the absence of ABA, metaphase I and metaphase II cell
177 populations peak at approximately 75 and 120 min, respectively, as determined by spindle
178 morphology (Figure 1C). Addition of abscisic acid (ABA) at prophase release extended
179 metaphase I by 15 minutes and metaphase II by 30 minutes (Figure 1C). This suggested that
180 conditional dimerization of Spc105$^{(1-455)}$-PYL and Mps1$^{(440-765)}$-ABI is sufficient to activate the
181 SAC and delay cells in either metaphase I or metaphase II. To delay cells specifically at
182 metaphase II, we added ABA at 100 minutes after prophase release, corresponding to the
183 anaphase I peak according to spindle morphology, and this resulted in a pronounced (60 min)
184 metaphase II delay (Figure 1C).
185 To confirm that the delay in cell cycle progression was dependent on the canonical
186 spindle checkpoint cascade, we tested whether the SynSAC-induced metaphase delays
187 required downstream SAC proteins. Unlike the control SynSAC strain, we observed no delays
188 in the metaphase to anaphase transitions when Mad1, Mad2, or Mad3 were absent (Figure
189 1D). Similarly, SynSAC dimerization after meiosis I did not delay cells in metaphase II in the
190 absence of the SAC proteins (Supp Figure 1A). Therefore, both meiotic metaphase delays
191 induced by dimerization of Mps1$^{(440-765)}$-ABI and Spc105$^{(1-455)}$-PYL are dependent on known
192 downstream SAC components. We conclude that SynSAC can induce a delay in both
193 metaphase I and metaphase II.
194
195 **Metaphase I, metaphase II and mitotic metaphase show differential sensitivity to**
196 **SynSAC**
197 We noticed that SynSAC induced a more pronounced delay in metaphase II than metaphase
198 I (Figure 1C and D; Supp Figure 1). Furthermore, both the metaphase I and metaphase II
199 arrests were transient and cells subsequently underwent both meiotic divisions to produce
200 spores, even in the presence of ABA. In contrast, SynSAC induced a robust mitotic metaphase
201 arrest and checkpoint-dependent growth inhibition (Supp Figure 2A and B). This is in
202 accordance with findings in yeast and vertebrates which have suggested that the SAC is less
203 robust in meiosis I compared to either mitotic metaphase or metaphase II (Gui & Homer, 2012;
204 Nagaoka *et al*, 2011; Kolano *et al*, 2012; Lane *et al*, 2012; MacKenzie *et al*, 2023; Sebestova
205 *et al*, 2012). However, since these previous observations rely on methods which perturb
206 kinetochore-microtubule attachments, it has remained unclear whether this difference stems
207 from reduced SAC signalling or a dampened response. Our finding that SynSAC, which

208 uncouples signal generation from the response, induces a graded effect, demonstrates that
209 meiosis I and to a lesser extent meiosis II have a reduced response to checkpoint signalling.
210 To explore the differences between the meiosis I and II SAC responses further, we
211 analysed the effects of SynSAC on downstream signalling events. The SAC inhibits the APC-
212 Cdc20 from targeting the anaphase inhibitor securin for degradation. Therefore, we monitored
213 Pds1^{securin} degradation as a readout for APC-Cdc20 activity in the SynSAC strain. Without
214 ABA-induced dimerization, Pds1^{securin} levels decreased along with the appearance of
215 anaphase I spindles at 90 minutes after prophase release, re-accumulated at 105 minutes,
216 then decreased again at 135 minutes when anaphase II spindles appeared (Figure 2A).
217 Addition of abscisic acid (ABA) at the time of prophase release slightly attenuated the
218 decrease in Pds1^{securin} levels at 90 minutes, consistent with induction of a modest metaphase
219 I delay. As before, spindle morphology indicated a more pronounced metaphase II delay
220 compared to metaphase I, and, consistently, Pds1^{securin} remained stabilised even after
221 metaphase II spindle disappearance at 165 minutes (Figure 2B). Therefore, SynSAC
222 activation prior to metaphase I stabilises Pds1^{securin} with the greatest effect in meiosis II. When
223 ABA was added after metaphase I at 100 minutes after release, Pds1^{securin} levels similarly
224 remained high until the end of the timecourse and after spindle disassembly (Figure 2C).
225 Together, these findings suggest that activation of the SynSAC in meiosis delays metaphase
226 I and II by preventing Pds1^{securin} degradation. Interestingly, although SynSAC induces a longer
227 delay in metaphase II compared to metaphase I, in both cases the delay is transient and
228 accompanied by Pds1^{securin} persistence.
229 One possibility for the extended delay in metaphase I compared to metaphase II could
230 be differential protein expression in the two divisions. To test this, we assessed the levels of
231 the SynSAC dimerising proteins by Western blotting. Both full length endogenous and the C-
232 terminal SynSAC fragment of Mps1 were tagged with 3V5 for direct comparison, which
233 revealed increased expression of Mps1$^{(440-765)}$-ABI-3V5 compared to Mps1-V5 (Supp Figure
234 3A- B), consistent with the presence of a degron in the N-terminal domain of Mps1 (Palframan
235 *et al*, 2006). However, levels of the SynSAC Mps1$^{(440-765)}$-ABI-3V5 fragment were relatively
236 consistent throughout meiosis I and II (Supp Figure 3A-B). Similarly, FLAG-tagging of both full
237 length endogenous Spc105 and Spc105$^{(1-455)}$-PYL indicated that protein levels were
238 equivalent across the two divisions (Supp Figure 3C-D). Thus, differences in the abundance
239 of the SynSAC dimerising constructs cannot account for the longer delay in metaphase I
240 compared to metaphase II.
241 Finally, the transience of the SynSAC delay at both metaphase I and metaphase II
242 raised the question of whether escape into anaphase I and II was associated with accurate

243 chromosome segregation. We further sought to confirm that the SynSAC constructs we
244 engineered to avoid kinetochore localisation did indeed not disrupt kinetochore function. To
245 test this, SynSAC strains were allowed to complete sporulation in the presence of ABA and
246 spore viability was measured. If kinetochores or chromosome segregation were significantly
247 disrupted by the delayed meiotic cell cycle, spores would inherit the incorrect number of
248 chromosomes and be inviable. However, spore viability after SynSAC dimerization, either
249 before metaphase I or specifically in metaphase II, was not significantly different from wild
250 type (Supp Figure 2C). Therefore, SynSAC does not disrupt chromosome segregation and
251 provides a powerful tool to study meiotic metaphase.
252
253 ***PP1 binding to Spc105 limits SAC-induced metaphase delay in meiosis***
254 Why does SynSAC induce a more potent arrest in metaphase II compared to metaphase I?
255 One possibility is that checkpoint silencing mechanisms are especially active in meiosis I and
256 could contribute to a rapid reversal of the checkpoint activity. A key event in checkpoint
257 silencing is the docking of Protein Phosphatase 1 (PP1; Glc7 in yeast) onto two consensus
258 motifs in the N-terminal region of Spc105, leading to the dephosphorylation of Spc105 and the
259 disassembly of the SAC signalling platform (Rosenberg *et al*, 2011; Roy *et al*, 2019). Analysis
260 of mitotic cells indicated that the RVxF motif is the primary PP1 docking motif and that the
261 SILK motif (GILK in budding yeast) plays an auxiliary role (Rosenberg *et al*, 2011; Roy *et al*,
262 2019). To test whether PP1 binding to Spc105 regulates the duration of the SynSAC delay in
263 meiosis, we created strains in which the dimerizing copy of Spc105$^{(1-455)}$-PYL in the SynSAC
264 strain background had mutations in the RVxF and SILK motifs that would prevent PP1 binding.
265 We mutated either the SILK motif, creating *spc105$^{(1-455)}$-4A-PYL*, or the RVSF motif, creating
266 *spc105$^{(1-455)}$-RASA-PYL*, and additionally generated *spc105$^{(1-455)}$-4A-RASA* which has both
267 PP1-binding motifs mutated. We also made the *spc105$^{(1-455)}$-RVAF* mutant in which S77 within
268 the RVSF motif is mutated to alanine, to block potential Ipl1$^{\text{Aurora B}}$ phosphorylation of this site.
269 In human cells, Aurora B-dependent phosphorylation of KNL1S$^{\text{Spc105}}$ within the RVSF motif
270 appears to prevent PP1 binding (Liu *et al*, 2010). However, the phospho-null RVAF mutant
271 does not impact growth of budding yeast, suggesting it may not have as much importance in
272 this organism (Rosenberg *et al*, 2011; Roy *et al*, 2019).
273 In the absence of ABA, mutation of the PP1 binding sites in the SynSAC construct did
274 not affect meiotic progression or spore viability (Supp Fig 4A and B), nor did they compromise
275 mitotic growth (Supp Figure 4C). However, activating the SynSAC by adding ABA at the time
276 of prophase release resulted in a metaphase I delay of varying duration depending on the
277 status of the PP1-binding motifs (Figure 3A). Mutation of the SILK motif (*spc105$^{(1-455)}$-4A*) did

278 not detectably alter the 15-30 min metaphase I delay observed for the wild-type SynSAC
279 (Figure 3A), consistent with the notion that this motif is less important. However, preventing
280 PP1 binding to the RVxF motif (*spc105*$^{(1-455)}$*-RASA*) extended the duration of the SynSAC-
281 induced metaphase I delay considerably and mutation of both PP1 binding motifs (*spc105*$^{(1-}$
282 $^{455)}$*-4A-RASA*) led to an even more pronounced delay, with metaphase I cells persisting until
283 the end of the timecourse (Figure 3A). Conversely, mutation of the potential Ipl1$^{\text{Aurora B}}$-
284 dependent kinase site (*spc105*$^{(1-455)}$*-RVAF*), which is predicted to increase PP1 binding and
285 thereby promote checkpoint silencing, modestly decreased the duration of the metaphase I
286 delay (Figure 3A). Taken together, these findings indicate that PP1 binding to Spc105
287 dampens the SynSAC response in meiosis I and that both PP1 binding motifs play a role, with
288 the RVxF motif being the primary binding site.
289 To test whether the duration of the metaphase II delay is also affected by the ability of
290 PP1 to bind Spc105, we repeated the above experiment except ABA was added only at the
291 time of anaphase I. As for metaphase I, preventing PP1 binding to Spc105 increased the
292 duration of SynSAC-induced metaphase II, with the different mutations showing a gradient of
293 effects (Figure 3B). The strongest metaphase II delay was observed with the *spc105*$^{(1-455)}$*-4A-*
294 *RASA* construct, with the *spc105*$^{(1-455)}$*-RASA* mutant alone also extending metaphase II
295 compared to the wild-type, as judged by the absence of anaphase II cells. Mutation of the
296 SILK motif (*spc105*$^{(1-455)}$*-4A*) caused a modest additional 15 minutes delay. However, we
297 observed no detectable effect of mutating the potential Ipl1$^{\text{Aurora B}}$ site on the SynSAC
298 metaphase II delay (Figure 3B). Overall, these results indicate that PP1 binding to the RVxF
299 motif, and to a lesser extent the SILK motif, on Spc105 affects the duration of the metaphase
300 to anaphase transition in both meiosis I and II. Interestingly, the effect on metaphase I appears
301 more striking, potentially suggesting increased PP1-dependent SAC silencing activity in
302 meiosis I.
303
304 ***Kinetochore composition changes at meiotic prophase, metaphase I, and metaphase II***
305 The SynSAC system we developed allows robust isolation of populations of both metaphase
306 I and metaphase II cells from the same strain, providing the first opportunity for biochemical
307 comparisons between these stages. As proof-of-principle, we analysed kinetochores, which
308 must be modified to achieve distinct functions during meiosis. Indeed, previous work has
309 established a dramatic remodelling of kinetochore composition between meiotic prophase and
310 meiosis I (Meyer *et al*, 2015; Borek *et al*, 2021). However, the lack of a suitable arrest system
311 precluded analysis of meiosis II. Since kinetochores undergo a configuration switch from
312 mono-oriented in meiosis I to bi-oriented in meiosis II to direct the successive segregation of

313 homologs and sister chromatids, direct comparison of meiosis I and meiosis II kinetochores is
314 an important goal. We exploited our newly developed SynSAC system to determine
315 kinetochore composition at metaphase I and metaphase II, together with mitotic metaphase
316 and meiotic prophase for comparison. To do so, we purified kinetochores via
317 immunoprecipitation of the central kinetochore protein Dsn1 and used mass spectrometry to
318 analyse their composition (Akiyoshi *et al*, 2010; Sarangapani *et al*, 2014; Borek *et al*, 2021).
319 Metaphase arrests were confirmed by spindle immunofluorescence (Supp Fig 5A) and silver
320 staining indicated broadly similar purifications across replicates and cell cycle stages (Supp
321 Fig 5B).

322 To determine kinetochore composition, we used data independent acquisition (DIA)
323 mass spectrometry. Due to the high sensitivity of this method, thousands of proteins were
324 quantified in each of three replicate immunoprecipitations from each stage (Supp Figure 6A)
325 and 2,415 quantified proteins were common to all three replicates of the Dsn1-His-FLAG IPs
326 from all 4 cell cycle stages (Supp Figure 6A-B). As expected, Dsn1 and other components of
327 the core kinetochore structure, especially other members of the KMN (KNL1^{Spc105}-Mis12^{MIND}-
328 Ndc80) network were most enriched compared to the untagged control immunoprecipitations
329 (Supp Fig 6C-D). To better quantify differences in kinetochore protein abundances between
330 the different cell cycle stages, we scaled all protein abundances to the level of Dsn1 quantified
331 in each individual sample (Supp Fig 7A-D). As expected, the abundance of most kinetochore
332 proteins was slightly lower than the bait protein Dsn1 in *DSN1-His-Flag* ("tag") samples, but
333 not in the *DSN1* negative control immunoprecipitations ("no tag") (Supp Fig 7D). Overall, there
334 was an increased amount of quantified protein in the prophase and metaphase I kinetochore
335 ("tag") samples compared to the metaphase II and mitotic metaphase samples (Supp Fig 7E).
336 Although this difference was not significant when the levels of known kinetochore proteins
337 were compared (Supp Fig 7F), it is possible that it reflects increased stability of protein-protein
338 interactions with the kinetochore in prophase and metaphase I.

339 Next, we performed pair-wise comparisons to identify which proteins, relative to Dsn1,
340 were the most different in abundance between cell cycle stages (Supp Fig 8). In addition, we
341 used GO term analysis to identify shared functions among the top 50 non-kinetochore proteins
342 associated with the Dsn1 immunoprecipitate at each stage (Supp Fig 9A). At prophase,
343 proteins involved in chromosome pairing, recombination, and respiration were strongly
344 associated with kinetochores (Supp Fig 9A-B). At metaphase I, chromosome organization,
345 spindle pole body, and spindle organization proteins were enriched. The enrichment of many
346 chromatin-associated factors, e.g. histones and chromatin remodeling complexes, with
347 metaphase I, but not metaphase II kinetochores (Supp Fig 9B) is consistent with closer

348 association of kinetochores with chromatin in the mono-oriented vs bi-oriented state. At
349 metaphase II, sporulation and spore wall proteins became enriched (Supp Fig 9A-B). Mitotic
350 kinetochores were associated with nucleolar, ribosome, and nuclear envelope proteins (Supp
351 Fig 9A-B). Together, these associations underscore the dynamic nature of kinetochore protein
352 interactions. Further, it suggests that the kinetochore may serve as a platform to direct cell
353 cycle stage-specific signalling such as promoting recombination at meiotic prophase,
354 specialised kinetochore-spindle associations at metaphase I and instigating meiotic-exit
355 processes such as spore wall formation in metaphase II.

356 Beyond identifying novel protein interactions, we aimed to determine whether there
357 were significant changes in the kinetochore composition itself at the different stages, relative
358 to Dsn1. Across the 4 stages, we were able to quantify ~70 known kinetochore proteins (Figure
359 4A). As expected, proteins within the KMN network were most abundant, while proteins at the
360 inner or outer edges of the complex, or only transiently associated, were less abundant.
361 Comparing protein abundances grouped by sub-complex or function at each stage indicated
362 that inner kinetochore CCAN proteins were reduced at meiotic metaphase I and II compared
363 to prophase or mitotic metaphase, although the trend was not significant, while outer
364 kinetochore Dam1 complex proteins showed the reverse trend (Figure 4A-B). It is possible
365 that meiotic kinetochores are enriched in outer kinetochore complexes to facilitate the
366 challenge of capturing homologs in meiosis I. Alternatively, inner kinetochore protein
367 interactions may be weakened in the two meiotic metaphases, while outer kinetochore
368 interactions are better preserved during the purification. As expected, there was a significant
369 depletion of the Ndc80 and Dam1 complex proteins from kinetochores in prophase, in
370 agreement with previous observations (Miller *et al*, 2012; Chen *et al*, 2020; Hayashi *et al*,
371 2006; Meyer *et al*, 2015) (Figure 4A-B).

372 Within the diverse kinetochore "accessory" group, the strongest changes were an
373 enrichment of $Glc7^{PP1}$ phosphatase regulator Fin1 at meiotic metaphase I and II, as well as
374 an enrichment in $Glc7^{PP1}$ phosphatase at prophase. Additionally, proteins with known
375 functions in mono-orientation such as monopolin complex proteins Csm1 and Mam1 had
376 higher abundance or were exclusively detected in metaphase I but not metaphase II
377 kinetochores. SAC and CPC protein abundance on kinetochores was largely comparable in
378 all stages, other than a depletion in Mps1 levels at prophase, which likely reflects the fact that
379 this is the only condition in which SynSAC was not induced. Finally, microtubule-associated
380 proteins (MAPs) were relatively depleted from mitotic kinetochores and the $Bik1^{CLIP-170}$
381 microtubule plus-end tracking protein was particularly enriched on metaphase I and
382 metaphase II kinetochores, consistent with the general increase in abundance of the

383 microtubule-binding components of the outer kinetochore in these purifications (Figure 4A-B).
384 Together, our results reveal that although the levels of most core kinetochore proteins are
385 relatively stable at different cell cycle stages, there are significant differences. Notably, there
386 is a loss of outer kinetochore proteins at prophase, a depletion in some inner kinetochore
387 protein interactions at meiotic metaphase vs mitotic, and an increase in outer kinetochore
388 protein levels at metaphase I, and also to some extent at metaphase II.
389
390 ***Reduced phosphorylation of kinetochores at metaphase II***
391 Protein composition changes are only partially responsible for the distinct behaviour of
392 kinetochores in meiosis I and meiosis II. Indeed, multiple kinases are known to contribute (Lee
393 & Amon, 2003; Clyne *et al*, 2003; Petronczki *et al*, 2006; Matos *et al*, 2008; Lo *et al*, 2008),
394 indicating that phosphorylation is a key mechanism driving these changes. However, a global
395 picture of phosphorylation changes at the kinetochore is lacking. This is challenging because
396 phospho-peptides are relatively low in abundance and recovery of sufficient quantities of
397 protein from highly synchronised cells is especially important to detect changes between
398 stages. Our SynSAC approach makes this possible because large quantities of highly
399 synchronised cells can be collected within a single experiment.
400 To this end, 95% of the eluates from the kinetochore purifications above were
401 subjected to phospho-peptide enrichment and DIA-MS. Thus, alongside quantification of the
402 kinetochore-associated proteome as described above, we obtained matched phospho-
403 proteomic datasets for each sample. Overall, we identified 4,480 phosphorylation sites
404 ("phospho-sites") on 1,614 proteins with 99% confidence. The abundance of each phospho-
405 site was normalised to the total abundance of the corresponding protein quantified in the non-
406 phospho-enriched fraction of the sample. This more accurately identifies dynamic
407 phosphorylation, rather than protein abundance. Additionally, we filtered the dataset to
408 analyse only those phospho-sites which were identified in all replicates of at least one sample
409 type. With these metrics, we quantified ~1,500 phosphorylation sites on meiotic prophase and
410 meiotic metaphase I kinetochores and ~700-1,100 phospho-sites on meiotic metaphase II and
411 mitotic metaphase kinetochores (Supp Fig 10A). As expected, many phosphorylation sites
412 were stage-specific, with 177 sites identified in all replicates of all stages (Supp Fig 10B).
413 We performed GO term enrichment analysis to look for shared functions among the
414 phospho-proteins most abundant in the kinetochore purifications. This was done with the top
415 50 most abundant phospho-proteins which are not known kinetochore proteins, in order to
416 identify alternative processes. At prophase, phospho-proteins involved in chromosome
417 organization, double-strand break repair, and transcription were associated with kinetochores

418 (Supp Fig 10C). Similarly, metaphase I phospho-proteins were involved in chromatin
419 remodeling, chromosome organization, and gene expression. At metaphase II, phospho-
420 proteins involved in cell cycle regulation, sexual reproduction, and spindle pole body
421 organization were enriched (Supp Fig 10C). Finally, mitotic metaphase phospho-proteins were
422 involved in the microtubule cytoskeleton, nucleus organization, and regulation of transcription.
423 Overall, the temporal trends seen in the GO term analysis are apparent in ranked lists of the
424 most abundant non-kinetochore phospho-sites for each stage comparison (Supp Fig 10D).

425 To determine whether there were general trends in the total level of phosphorylation,
426 we analysed the distribution of kinetochore phospho-site abundances at the 4 different stages
427 (Figure 5A). The number of phospho-sites on known kinetochore proteins was around ~100
428 at each stage however the median level of phosphorylation was higher in meiotic prophase
429 and metaphase I than it was in metaphase II and mitotic metaphase (Figure 5A). This suggests
430 that kinetochores are subject to essential phosphorylation in meiosis I and that either
431 phosphatase activity increases, or kinase activity towards kinetochores decreases at
432 metaphase II. Interestingly, the total abundance of phosphorylation on kinetochores was very
433 similar between metaphase II and mitotic metaphase, suggesting that the increased level of
434 kinetochore phosphorylation is characteristic of meiosis I.

435 We next asked whether these phosphorylation events were focused on specific
436 kinetochore sub-complexes or functional groups. The CCAN and KMN subcomplexes
437 contained the most phosphorylation sites, while relatively few sites were mapped to the Cbf3
438 complex and MAPs (Figure 5A). The levels of phosphorylation on the CCAN and KMN
439 subcomplexes were highest in prophase and metaphase I, and lower in metaphase II and
440 mitotic metaphase, mirroring the trend seen for all kinetochore sites. Interestingly, there
441 appeared to be increased phosphorylation on outer kinetochore Dam1 complex proteins in
442 metaphase I vs II, and overall higher phosphorylation in meiosis vs mitosis. Since Dam1
443 complex proteins are known targets of error correction kinases Ipl1$^{\text{Aurora B}}$ and Mps1, this may
444 suggest increased error correction in meiosis vs mitosis. To identify which kinetochore
445 proteins were most phosphorylated, we calculated the sum of the abundance of all
446 phosphorylation sites on individual kinetochore proteins at each stage, and then ranked the
447 proteins based on the total sum from all stages (Figure 5B). This revealed that Spc105, Bir1,
448 Lrs4, Sli15, Dsn1, Okp1 and Ame1 were the most heavily phosphorylated kinetochore
449 proteins. Additionally, we determined the maximum range in abundance between cell cycle
450 stages for each phospho-site within each protein. This revealed that Mif2$^{\text{CENP-C}}$, Dsn1, Cin8$^{\text{Kif11}}$,
451 Okp1$^{\text{CENP-Q}}$, and Cse4$^{\text{CENP-A}}$ have highly dynamic phosphorylation sites (Figure 5C).

452 Finally, we highlight several individual phospho-sites with interesting trends (Figure
453 5D). Slk19^{CENP-F} regulates both spindle stability and mitotic/meiotic exit (Marston *et al*, 2003;
454 Stegmeier *et al*, 2002; Buonomo *et al*, 2003; Sullivan *et al*, 2001). We found that
455 phosphorylation of Slk19-S-23, in part of the protein involved in meiotic exit (Havens *et al*,
456 2010), is reduced in metaphase II. In mitosis, phosphorylation of the N-terminus of Ndc80 by
457 Ipl1$^{Aurora\ B}$ promotes detachment of kinetochores from microtubules, allowing for correction of
458 erroneous attachments (Pinsky *et al*, 2006; Akiyoshi *et al*, 2009; Sarangapani *et al*, 2013); in
459 meiosis, Ipl1$^{Aurora\ B}$ phosphorylation of an overlapping set of sites, including T54, destabilizes
460 Ndc80 protein levels in prophase, contributing to the loss of outer kinetochore proteins at this
461 time (Chen *et al*, 2020). Consistent with this, we observed significantly more phosphorylation
462 of Ndc80-T-54 on purified kinetochores in meiotic prophase and metaphase I (Figure 5D).
463 Dsn1-S-69 is found very close to where the monopolin complex that directs mono-orientation
464 in meiosis I is thought to bind (residues 72-110) (Sarkar *et al*, 2013; Plowman *et al*, 2019). We
465 observed greatest phosphorylation of Dsn1-S-69 in prophase and metaphase I, the time when
466 kinetochores prepare for mono-orientation, suggesting it may be a functionally important
467 modification (Figure 5D). Finally, we found that S70 phosphorylation on inner kinetochore
468 protein Okp1^{CENP-Q}, a likely Cdk substrate (Holt *et al*, 2009), is reduced at metaphase II.
469 To uncover trends in types of kinase activity directed towards kinetochore proteins,
470 we conducted motif analysis on phospho-sites at different cell cycle stages. Of the nearly 100
471 kinetochore phosphorylation sites identified, the most prominent trend was for a proline
472 residue at the +1 position from the phospho-acceptor site, which is a known motif recognised
473 by cyclin-dependent kinase (Cdk) (Figure 6A). Next, we analysed how many of the kinetochore
474 phospho-sites at each stage matched a panel of known kinase consensus motifs. The trends
475 were weak suggesting common types of kinase activity at the different stages, however, there
476 was a slight preference for the strict Cdk or Ipl1$^{Aurora\ B}$ kinase consensus motif among prophase
477 phospho-sites compared with the other stages (Figure 6B). Additionally, fewer sites matching
478 the Ipl1$^{Aurora\ B}$ motif were found in meiotic metaphase I and II (Figure 6B), which may suggest
479 that Ipl1$^{Aurora\ B}$ activity is reduced at these times. Indeed, we would anticipate that the prolonged
480 SynSAC arrest allows for robust chromosomal alignment and minimal requirement for Ipl1^{Aurora}
481 ^{B}-dependent error-correction. We previously found that, globally, Cdc5^{Polo} kinase promotes
482 phosphorylation of a more stringent motif of [DEN]x[ST]*F specifically in meiotic metaphase I
483 (Koch *et al*, 2024). We found that this trend also applies to kinetochores since the number of
484 phosphorylation sites on kinetochore proteins that match this motif was also highest at
485 metaphase I (Figure 6B). Finally, there was no stage-specific enrichment of the motif
486 recognised by the DDK kinase Cdc7, known to function in DNA damage repair and

487 homologous recombination in prophase (Figure 6B), suggesting that its activity is widespread
488 through mitosis and meiosis, or that other kinases can recognise these sites.
489 Given that the minimal Cdk and Cdc5^{Polo} kinase motifs were common among
490 kinetochore phospho-sites, we also analysed whether these sites were preferentially located
491 within specific sub-complexes. For Cdc5^{Polo} motif sites, this revealed a slight enrichment within
492 the outer kinetochore complexes KMN and Dam1c compared with the inner kinetochore
493 CCAN sub-complex, and this trend was most prominent at metaphase II and mitosis (Figure
494 6C). Conversely, at all stages there was an enrichment for Cdk motif sites within the inner
495 kinetochore CCAN complex vs the outer kinetochore KMN and Dam1 sub-complexes. Finally,
496 we reveal the identities of individual Cdc5^{Polo} and Cdk motif phospho-sites across the core
497 kinetochore (Figure 6D). There was a range of different trends, with some sites being
498 phosphorylated relatively equally across stages while others appeared enriched at specific
499 stages. Together, this dataset provides a strong basis for identifying phosphorylation sites
500 which may have key stage-specific roles such as directing mono-orientation in meiosis I and
501 biorientation in meiosis II.
502
503 **Discussion**
504 Mitosis, meiosis I and meiosis II involve distinct segregation events, each with specific
505 modifications to chromosome structure and orientation that must function in the context of a
506 unique cell cycle programme. Understanding these changes biochemically relies on the ability
507 to harvest cells at these distinct cell cycle stages for direct comparisons. Until now, meiosis II
508 has been particularly elusive since robust methods to arrest budding yeast cells in this stage
509 been lacking. However, meiosis II is of key interest: although it is often referred to as
510 "resembling mitosis", there are crucial differences since it occurs directly after another M
511 phase, meiosis I, and is followed by gamete formation. Here, we developed the SynSAC
512 system to overcome this limitation. SynSAC uses the same yeast strain to arrest cells in
513 metaphase of mitosis, meiosis I or meiosis II, allowing direct comparisons. This system could
514 be applied to interrogate changes in any cellular process or protein complex at these distinct
515 cell cycle stages. Here, as proof of principle, we determined the changes in protein
516 composition and phosphorylation abundance at kinetochores. Our findings develop a new tool
517 for meiotic investigations, provide key insights into meiotic regulation by SAC activation and
518 additionally generate an important resource that provides key insight into how kinetochores
519 are adapted at different cell cycle stages.
520
521 ***A simple method to arrest yeast cells at metaphase II***

522 We found that inducible dimerization of fragments of Spc105 and Mps1 upon prophase
523 release or during anaphase I allows for robust synchronization at metaphase I or II of meiosis,
524 respectively (Figure 1). Since the meiotic SynSAC method relies on two drug-inducible events
525 and does not require media washout steps, it greatly simplifies and improves recovery of
526 metaphase cells. SynSAC is also conditional, allowing the arrest to be induced only at the
527 desired time. This is in contrast to previous studies which have isolated metaphase I cells
528 through repressing transcription of *CDC20* (Lee & Amon, 2003), where loss of the Cdc20
529 protein may have secondary effects. Thus, by relying on relatively quick chemical reactions
530 and achieving arrest without reducing protein levels, the SynSAC method may more
531 accurately reflect the metaphase state.
532
533 ***PP1 restricts the duration of SAC signalling in metaphase I***
534 Interestingly, the duration of SynSAC-mediated delay is consistently shorter in meiosis I vs II,
535 despite equivalent protein level of the dimerizing construct. Microtubule-depolymerising drugs
536 also cause a shorter SAC delay in meiosis I compared to either meiosis II or mitosis
537 (MacKenzie *et al*, 2023). The differential sensitivity of cells to SynSAC in meiosis I and II
538 suggests that this is an intrinsic difference between the two divisions. Previous work has
539 established a role for PP1 in prematurely silencing the SAC in meiosis I in the presence of
540 improperly attached kinetochores (MacKenzie *et al*, 2023). Our work similarly implicates PP1
541 binding to Spc105 as being responsible for limiting the duration of the SynSAC arrest in
542 meiosis I. We discovered that mutation of either the conserved RVxF or the GILK motif does
543 indeed lengthen the duration of the metaphase I SynSAC arrest, with the strongest effect seen
544 when both mutations are present. This suggests that PP1 binding to these motifs may promote
545 Spc105 dephosphorylation and SAC silencing in metaphase I. Our system also allowed us to
546 directly test the effect of PP1 binding mutants in metaphase II, however we observed only
547 minor additional delays when PP1 binding to Spc105 was prevented. Together, these
548 observations suggest that PP1 activity is more prominent at metaphase I. How this relates to
549 the unique segregation pattern in this division where homologs, rather than sister chromatids,
550 are segregated is an important area of investigation for the future.
551 The stronger and more prolonged SynSAC arrest obtained using the PP1 binding site
552 mutant *spc105$^{1-455}$-4A-RASA* prompts its consideration as an alternative tool for future studies,
553 particular where meiosis I arrest is important. However, in the current study we found that the
554 wild type SynSAC protein fragments without these mutations yielded highly enriched
555 populations of metaphase I and II cells and reliable detection of kinetochore proteins and
556 phosphorylations expected to be specific to those stages.

557

558 ***Some inner kinetochore proteins are lost while outer kinetochore proteins are***
559 ***increased in meiosis vs mitosis***

560 We applied SynSAC to understand changes in composition of the kinetochore by quantitative
561 proteomic analysis. Prior work used Dsn1 kinetochore immunoprecipitations and
562 minichromosome purifications to compare kinetochore and centromere composition in mitosis,
563 prophase I and metaphase I (Borek *et al*, 2021). However, analysis of purified metaphase II
564 kinetochores was previously inaccessible and our application of high-sensitivity DIA mass
565 spectrometry, together with matched phosphorylation analysis, provides a more complete
566 picture overall. Our dataset of kinetochore composition from four stages: (1) mitotic
567 metaphase I; (2) meiotic prophase 1; (3) metaphase I and (4) metaphase II therefore greatly
568 extends our understanding of how kinetochores change during meiosis. Consistent with
569 remodelling reported in our earlier study (Borek *et al*, 2021), we reveal a change in the
570 stoichiometry of sub-complexes relative to each other, dependent on cell cycle stage. For
571 example, the inner kinetochore CCAN is less abundant at meiotic metaphase I and II
572 compared with mitosis and prophase (Figure 4A). The mechanisms underlying the lower
573 abundance of CCAN proteins, which notably include some of the most essential DNA-
574 contacting proteins such as the Cse4^{CENP-A} histone and the Ame1^{CENP-C}/Okp1^{CENP-Q}
575 heterodimer, during meiotic metaphase require further investigation. Moreover, it is possible
576 that this phenomenon contributes to the essential requirement for some CCAN proteins for
577 kinetochore assembly in meiosis, but not mitosis (Fernius & Marston, 2009; Borek *et al*, 2021;
578 Mehta *et al*, 2014). Conversely, we observed higher levels of Dam1 complex proteins at
579 meiotic metaphase I and II compared with mitosis, and this trend was significant for the
580 complex as a whole (Figure 4A-B). Along the same lines, there was a small but statistically
581 significant increase in the levels of KMN proteins in metaphase I specifically (Figure 4A-B).
582 Overall, there is a trend for a loss in inner kinetochore protein interactions and a gain in outer
583 kinetochore protein interactions in meiotic metaphase compared to mitotic metaphase. It is
584 tempting to speculate that kinetochores are more loosely associated with chromatin and more
585 strongly associated with the spindle through the outer kinetochore in meiotic vs mitotic
586 metaphase. Potentially, kinetochore-spindle interactions are stabilised to better ensure
587 accurate segregation during the rapid metaphase-anaphase transitions of meiosis and to cope
588 with the challenging configuration of homologs in meiosis I, relying on chiasmata-dependent
589 linkages.

590

591 ***Metaphase II kinetochores have reduced phosphorylation***

592 Our phospho-proteomic analysis of purified kinetochores from meiosis and mitosis identified
593 4,487 phosphorylation sites on 1,614 proteins, indicating that ~35% of the detected proteome
594 is phosphorylated, in agreement with previous studies (Supp Figure 10) (Wettstein *et al*, 2024;
595 Ptacek *et al*, 2005). Nearly twice as many phospho-sites were identified in meiotic prophase
596 and metaphase I compared with metaphase II and mitotic metaphase (Supp Figure 10).
597 Around 250-400 more proteins were detected in prophase and metaphase I, suggesting
598 unique regulation at the level of protein abundances as well as phosphorylation (Supp Figure
599 7E). We found less variation in the number of phospho-sites found on known kinetochore
600 proteins, with around 100 sites identified on ~70 kinetochore proteins across all stages (Figure
601 5A). Despite this similarity, we quantified significant differences in the overall abundances of
602 the phospho-sites, with meiotic prophase and metaphase I kinetochores having significantly
603 higher levels of phosphorylation compared with meiotic metaphase II and mitotic metaphase
604 (Figure 5A). Within the core kinetochore structure, most phospho-sites mapped to the
605 chromatin-associated CCAN or the spindle-associated KMN complexes. It seems highly likely
606 that some of these phosphorylation events are important for the unique mono-oriented
607 arrangement of sister chromatids in meiosis I, and future research should aim for their
608 functional characterisation.
609 Furthermore, most of the detected phosphorylation sites were unique to the stage and
610 therefore their function is likely to be stage-specific (Supplementary Figure 10B). Whether
611 sister kinetochore biorientation at metaphase II and mitotic metaphase is physically and/or
612 biochemically distinct remains unclear. Our characterisation of meiotic SynSAC duration and
613 previous work with the endogenous SAC (MacKenzie *et al*, 2023) suggest that metaphase II
614 is regulated differently, with metaphase II having a shorter arrest compared to mitotic
615 metaphase upon SynSAC activation. However, previous biophysical characterisation
616 indicated that the kinetochore-microtubule attachment strength of metaphase II and mitotic
617 purified kinetochores was equivalent on average (Sarangapani *et al*, 2014). Thus, it may be
618 that the shorter duration of metaphase II does not depend on maximum attachment strength
619 per se and rather on some intrinsic cell cycle regulation or other properties of kinetochores in
620 these stages. Indeed, the distance between sister centromeres in mouse metaphase II
621 oocytes is nearly double that in human and mouse mitotic cells, so there are likely biophysical
622 differences between biorientation at these two stages (Kouznetsova *et al*, 2019). Additionally,
623 as many as ~20% of chromosomes in mouse metaphase II cells appear to have lateral or
624 merotelic attachments that persist into anaphase II, when they are then corrected
625 (Kouznetsova *et al*, 2019). Thus, compared with mitosis, error-correction mechanisms are
626 notably different in meiosis. Error-correction relies on phospho-regulation of the outer

627 kinetochore sub-complexes KMN and Dam1c, and we observed higher levels of Dam1
628 complex proteins in kinetochores from meiosis vs mitosis. This, in addition to the differential
629 phospho-sites identified on outer kinetochore proteins, provides a good first step for future
630 investigations into meiotic kinetochore attachment mechanisms and how they differ in meiosis
631 I and meiosis II.
632
633
634 **Materials and Methods**
635
636 ***Plasmids***
637 Plasmids used in this study are listed in Supplemental Table 1.
638 *MPS1(440-765)* in a *HIS3* single integration plasmid AMp1725 was made by restriction
639 digest of empty *HIS3* single integration plasmid AMp1694 (received from Biggins Lab) and
640 *MPS1(440-765)* amplified from wild type SK1 yeast genomic DNA. *pMPS1-MPS1(440-765)* in
641 a *HIS3* single integration plasmid AMp1740 was made by Gibson assembly of ~500bp of
642 *MPS1* promoter amplified from wild type SK1 yeast genomic DNA and AMp1725. *pMPS1-*
643 *MPS1(440-765)-AB*I in a *HIS3* single integration plasmid AMp1755 was made by Gibson
644 assembly of ABI amplified from AMp1460 (received from Hardwick Lab, made in Heun Lab)
645 and AMp1740.
646 *pSPC105-SPC105(1-455)-PYL-3FLAG* in a *LEU2* single integration plasmid AMp1741
647 was made by Gibson assembly of 3 parts. ~500bp of *SPC105* promoter and *SPC105(1-455)*
648 were amplified from wild type SK1 genomic DNA, *PYL-3FLAG* was amplified from plasmid
649 AMp1461 (received from Hardwick Lab, made in Heun Lab) and *LEU2* single integration
650 plasmid AMp1697 (received from Biggins Lab).
651 *pSPC105-SPC105(1-455)-PYL* in a *LEU2* single integration plasmid AMp2055 was
652 made by megaprimer mutagenesis (two-step PCR) to completely remove the 3FLAG tag in
653 AMp1741.
654 PP1 binding site mutations in *SPC105-PYL* plasmids were made by megaprimer
655 mutagenesis. *spc105(1-455)-4A* mutates the 21-GILK-24 motif to 21-AAAA-24. *spc105(1-*
656 *455)-RASA* mutates the 75-RVSF-78 motif to 75-RASA-78. The *spc105(1-455)-4A-RASA*
657 plasmid contains both sets of mutations. *spc105(1-455)-RVAF* mutates serine 77 to alanine
658 only.
659
660 ***Yeast strains***

661 Budding yeast strains used in this study were derivatives of SK1 and are listed in
662 Supplemental Table 2. *pGAL1-NDT80 pGPD1-GAL4.ER* was described previously (Benjamin
663 *et al*, 2003). The *MPS1-3V5*, *SPC105-6His-3Flag*, and *DSN1-6His-3Flag* strains were made
664 by standard PCR tagging methods. SynSAC strains with *MPS1(440-765)-ABI* and *SPC105(1-*
665 *455)-PYL* integrated at the *his3* and *leu2* locus, respectively, were made by restriction
666 digestion of the appropriate plasmids and standard yeast DNA transformation procedures.
667 Yeast strains are available upon request without restriction.
668
669 ***Meiotic prophase block-release timecourse***
670 Cells were induced to undergo meiosis as described by (Barton *et al*, 2022) and *pGAL-*
671 *NDT80* prophase block-release experiments were performed as outlined in (Carlile & Amon,
672 2008). Briefly, strains were patched from –80 °C stocks to YPG agar (1% Bacto yeast extract,
673 2% Bacto peptone, 2.5% glycerol, 0.3 mM adenine, 2% agar) plates. After ~16 h, cells were
674 inoculated into YPDA media and grown for 24 h at 30 °C with shaking at 250 rpm. Next,
675 BYTA (1% Bacto yeast extract, 2% Bacto tryptone, 1% potassium acetate, 50 mM potassium
676 phthalate) cultures were prepared to OD_{600} = 0.3 and grown at 30 °C with shaking at 250 rpm
677 overnight (~16 h). The next morning, cells were washed twice in sterile water and resuspended
678 in sporulation medium (0.3% potassium acetate, pH=7.0) at OD_{600} = 2.0. After 5.5 h in
679 sporulation media, 1 µM β-estradiol was added to release cells from prophase and samples
680 were collected for immunofluorescence every 15 min until 180 min, and then every 30 min for
681 a further hour. For experiments where protein samples were analysed by Western blotting, 10
682 ml of meiotic culture or 5 ml of mitotic culture was collected by centrifugation and resuspended
683 in 5 ml ice-cold 5% trichloroacetic acid (TCA). Cells were collected again by centrifugation and
684 transferred to Fastprep (MP) tubes. Cell pellets were snap frozen in liquid nitrogen and stored
685 at -70 °C. Frozen cell pellets were washed in 500 µl acetone and air-dried. Cell pellets were
686 resuspended in TE with 2.75µM DTT and 1x Roche cOmplete protease inhibitor cocktail.
687 Protein samples were prepared by bead-beating in an MP Fastprep machine, at speed 6.5 for
688 3 rounds of 45 seconds with 1 min on ice in between, at 4 °C. SDS Sample buffer was added
689 (final concentration 3% SDS) and samples were boiled for 3 minutes before PAGE.
690
691 ***Spore viability assay***
692 All spore viability assays were carried out following prophase block-release timecourses.
693 Following the timecourse, cultures were left shaking at 30 °C ~24h. 100ul of culture was
694 collected by spinning in a microcentrifuge for 1min 13k rpm and then resuspended in 20ul
695 1mg/ml zymolyase in 1M sorbitol and incubated for 10 minutes at room temperature before

696 adding 1mL sterile water. Tetrads were dissected with a micromanipulator on a Nikon Eclipse
697 50i light microscope.
698
699 ***Mitotic alpha factor arrest-release timecourse***
700 Yeast strains were patched from –80 °C stocks to YPG agar (1% Bacto yeast extract, 2%
701 Bacto peptone, 2.5% glycerol, 0.3 mM adenine, 2% agar) plates. The next day, strains were
702 patched to YPDA (1% Bacto yeast extract, 2% Bacto peptone, 2% glucose, 0.3mM adenine)
703 agar plates. The next day, cells were inoculated into YPDA medium and grown overnight ~16h
704 at 30 °C with shaking at 250 rpm. The next morning, cultures were diluted to OD ~0.2 and
705 grown for 2 hours at room temperature with shaking at 250 rpm. Cultures were diluted back
706 to OD ~0.2 and alpha factor was added to 7.5 µg/ml. Cultures were shaken at room
707 temperature for 3 hours before checking that >90% of cells were shmooing or unbudded. Cells
708 were washed three times in 2x volume water and collected by centrifuging in a tabletop
709 centrifuge 3k rpm for 2 minutes at room temperature. Cells were resuspended in fresh YPDA
710 and placed into clean flasks. Culture samples of 100µl were taken at time zero before addition
711 of either ethanol or 250 µM abscisic acid (ABA) and then at 30 minute intervals after addition
712 of ethanol or ABA. 100ul culture samples were immediately combined with 400µl ethanol and
713 stored at 4 °C. For DNA staining, cells were pelleted and resuspended in 100ul 1 µg/ml DAPI
714 in PBS. Yeast cells were sonicated for 30 seconds on low in a Bioruptor Twin sonicating device
715 (Diagenode) and glass slides were prepared and visualised on a Zeiss Axioplan Imager Z2
716 fluorescence microscope with a 100x Plan ApoChromat NA 1.45 oil lens. At least 100 cells
717 were counted for each condition.
718
719 ***Serial dilution mitotic growth assay***
720 Yeast strains were inoculated into YPDA medium and grown overnight ~16h at room
721 temperature. Cultures were diluted to OD_{600}=0.2 and grown to mid-log at room temperature
722 before being diluted back to OD_{600}=0.3. Serial dilutions were set up in 96-well plates, with 5-
723 fold dilutions across rows. Yeast were transferred to YPDA plates or YPDA plates spread with
724 250 µM abscisic acid (ABA). Plates were incubated at 30 °C for ~24 h before taking images.
725
726 ***Spindle immunofluorescence***
727 Meiotic spindles were visualised by indirect immunofluorescence as described in (Barton *et*
728 *al*, 2022). A rat anti-tubulin primary antibody (AbD serotec) at 1:50 dilution and an anti-rat FITC
729 conjugated secondary antibody (Jackson Immunoresearch) at 1:100 dilution were used. A
730 Ziess Axioplan Imager Z2 fluorescence microscope with a 100x Plan ApoChromat NA 1.45 oil

731 lens was used to visualise cells. In total, 100-200 cells were counted at each timepoint and/or
732 for each sample.
733
734 ***SDS-PAGE and Western blotting***
735 SDS-PAGE and Western blotting were carried out largely as described in (Barton *et al*, 2022),
736 with minor modifications. Protein samples were separated on 10% bis-tris acrylamide gels
737 submerged in running buffer (25 mM Tris, 190 mM glycine, 0.01% SDS) using the Bio-Rad
738 Mini-Protean or Scie-plas TV200Y wide format mini gel system. SDS-PAGE gels were
739 transferred onto nitrocellulose membrane (0.45uM, Amersham-GE Healthcare) in transfer
740 buffer (25 mM Tris, 1.5% glycine, 0.02% SDS, 10% methanol) in a Bio-Rad Mini Trans-Blot
741 system or a semi-dry Amersham TE70 transfer unit.
742 Membranes were blocked in 5% milk in PBS with 0.01% Tween-20 (PBST) for at least
743 30 minutes before incubation in primary antibody overnight with gentle shaking at 4 °C. At
744 room temperature, membranes were washed three times for 10 minutes in PBST before
745 incubation in secondary antibody for 1 hour. Membranes were washed for 10 minutes, 3 times,
746 before visualisation using chemiluminescence. HRP-conjugated antibodies were detected
747 with ECL blotting substrate (Pierce), SuperSignal West Pico Plus substrate (Pierce), or
748 SuperSignal West Atto substrate (Pierce) for weaker signals and images were acquired with
749 a ChemiDoc MP Imaging System (Bio-Rad).
750
751 ***Growth conditions for kinetochore immunoprecipitations***
752 All immunoprecipitations were performed with lysate from either a *DSN1-His-Flag*
753 strain (33675) or no tag *DSN1* (30990) strain grown in different conditions.
754 For each replicate from meiotic cultures, two cultures of 400mL OD~2.0 were
755 sporulated in 4L flasks and scored for metaphase arrest by spindle IF as appropriate. Cultures
756 that were most similar by date of growth and spindle IF were combined during later grinding
757 lysis. For each replicate from mitotic cultures, 800ml OD=1.1-1.3 culture was grown in one 4L
758 flask and harvested and processed together.
759 For each 400mL meiotic culture, strains were patched from -70 stocks to YPG plates
760 and grown at 30C. After ~24h, a 25mL YPDA culture in a 250 mL flask was inoculated and
761 grown at 30C, shaking at 250 rpm. After ~24h, a 200mL BYTA culture in a 2L flask was started
762 at OD=0.2 and grown at 30C, shaking at 250rpm. The next morning, after ~16h, a 400ml
763 culture in a 4L flask was started at OD~2.0 in sporulation medium. All meiotic cultures were
764 grown at 30C with shaking at 250rpm. For meiotic prophase, cultures were incubated for 5.5
765 hours before harvest. For metaphase I, cultures were incubated for 5.5 hours before 1 μM β-

766 estradiol and 250uM ABA were added together. After 90 minutes, cells were harvested. For
767 metaphase II, cultures were incubated for 5.5 hours before 1 µM β-estradiol was added. After
768 105 minutes, 250 µM ABA was added and cells were harvested at 135 minutes. Samples for
769 spindle immunofluorescence were collected at the time of harvest.
770 For each mitotic culture, strains were patched from -70 stocks to YPG plates and grown
771 at 30C. After ~24h, a 25mL YPDA culture was inoculated in a 125mL flask and grown at 30C
772 with shaking at 250rpm. After ~16h, an 800 mL YPDA culture was started in a 4L flask at
773 OD~0.3 and grown at 30C with shaking at 250rpm. After ~3h, the OD=1.1-1.2 culture was
774 harvested.
775
776 ***Immunoprecipitation of kinetochores for mass spectrometry***
777 Immunoprecipitations were carried out essentially as described in (Borek *et al*, 2021),
778 with minor modifications.
779 *Harvest:* Cell cultures were spun at 4k rpm for 5 min at 4C in a Beckman Avanti J25
780 centrifuge. Each 400ml cell culture pellet was washed in 150 mL water and spun again the
781 same way. Then, cell pellets were resuspended in BH0.15 lysis buffer (150mM KCl, 25mM
782 HEPES-KOH pH 8.0, 2mM MgCl2, 0.5mM EGTA-KOH pH 8.0, 0.1mM EDTA-KOH pH 8.0,
783 0.1% NP-40) including phosphatase inhibitors (5mM NaF, 2mM Na-beta-glycerophosphate,
784 1mM sodium pyrophosphate, 800uM sodium orthovanadate, 200nM microcystin-LR) and
785 protease inhibitors (2mM Pefabloc, 10ug/ml each of 'CLAAPE' (Chymostatin,
786 Leupeptin,Aprotinin,Antipain,Peptstatin A,E-64), and 1x Roche cOmplete inhibitor cocktail).
787 Cell pellets were resuspended in BH0.15 including inhibitors according to the following
788 equation: OD600 x culture volume in L x 2 = mL buffer (ie for each 400 mL OD=2.0 pellet,
789 cells were resuspended in 1.6mL buffer). Resuspended cultures were drop frozen into liquid
790 nitrogen and stored at -70 before further processing.
791 *Lysis:* Frozen cell pellets were lysed by cryo-grinding in a SPEX 6875 Freezer Mill,
792 with 5 min pre-cool, 2 min Run time, 2 min Cool time, 8 cycles of 10 cycles per second. Cryo-
793 grindate was stored at -70 before further processing.
794 *Antibody conjugation to Dynabeads:* As described in (Borek *et al*, 2021). Antibody-
795 conjugated Protein G Dynabeads (ThermoFisher) were always prepared no more than 24
796 hours before use and were stored at 4 C until use.
797 *Immunoprecipitation and elution:* Grindate powder, in 50mL falcons, was thawed in
798 room temperature water before transferring to ice. Thawed grindate was clarified by
799 centrifugation in a tabletop centrifuge at 3,500 rpm for 10 min 4C. The supernatant, the lysate,
800 was transferred to a new falcon tube and concentration measured by standard Bradford Assay

801 (BioRad Cat#5000006). IPs were set up so that 80-100mg protein was incubated with ~100
802 uL anti-FLAG conjugated Protein G Dynabeads (ThermoFisher). The ratio of protein to beads
803 was always kept such that 12.6 mg protein was incubated with 15 uL antibody-conjugated
804 beads. IPs of replicates of the same condition were all done on the same day and normalised
805 so that protein concentration and antibody-bead volumes were the same between replicates.
806 Protein lysates and antibody-conjugated Dynabeads were incubated together in falcon tubes
807 with gentle rotation at 4C for 3 hours. Next, supernatants were collected and beads were
808 washed twice in 1mL BH0.15 with phosphatase and protease inhibitors by gently inverting the
809 tubes, then washed once in 1mL BH0.15 alone. Protein was eluted from beads in two rounds
810 of 10 min at 50C in a ThermoMixer C (Eppendorf) at 500-600 rpm with 0.1% RapiGest SF in
811 50mM Tris pH 8.0, added to one-half volume of Dynabeads (ie two rounds of 50 ul elution for
812 100 ul Dynabeads). The two sequential elutions were combined and the eluate was stored at
813 -70 before further processing.
814
815 ***Silver staining***
816 Protein samples were separated on 4-12% NuPAGE pre-cast gels (Invitrogen) run in MES
817 buffer (50mM MES, 50mM Tris Base, 0.1% SDS, 1mM EDTA, pH 7.3) and stained using an
818 Invitrogen Silverquest staining kit following the manufacturer's instructions.
819
820 ***Preparation of samples for mass spectrometry***
821 RapiGest eluates were prepared for mass spectrometry by trypsin digestion with a
822 filter-aided sample preparation (FASP) method, essentially as described in (Wiśniewski *et al*,
823 2009; Koch *et al*, 2024).
824
825 ***Phospho-peptide enrichment***
826 For each trypsin-digested peptide solution, 5% was loaded directly onto C18 stage
827 tips, called the "N" sample, and 95% was processed for phospho-peptide enrichment via Ti-
828 IMAC beads (MagReSyn) as described in (Koch *et al*, 2024), and called the "PE" (for phospho-
829 enriched) sample before loading on C18 stage tips. Samples of the same condition were all
830 processed on the same day (eg all prophase samples were processed together on the same
831 day).
832
833 ***DIA mass spectrometry***
834 The "N" and "PE" peptides eluted from the filter units were acidified using 20 μl of 10%
835 Trifluoroacetic Acid (TFA) (Sigma Aldrich). Samples were spun onto StageTips as described

836 by (Rappsilber *et al*, 2007). Peptides were eluted in 40 µL of 80% acetonitrile in 0.1% TFA
837 and concentrated down to 1 µL by vacuum centrifugation (Concentrator 5301, Eppendorf, UK).
838 They were then prepared for LC-MS/MS analysis by diluting it to 5 µL by 0.1% TFA.
839 LC-MS analyses were performed on Orbitrap Exploris™ 480 (Thermo Fisher Scientific,
840 UK) on a Data Independent Acquisition (DIA) mode, coupled on-line, to an Ultimate 3000
841 HPLC (Dionex, Thermo Fisher Scientific, UK). Peptides were separated on a 50 cm (2 *µ*m
842 particle size) EASY-Spray column (Thermo Scientific, UK), which was assembled on an
843 EASY-Spray source (Thermo Scientific, UK) and operated constantly at 55°C. Mobile phase
844 A consisted of 0.1% formic acid in LC-MS grade water and mobile phase B consisted of 80%
845 acetonitrile and 0.1% formic acid. Peptides were loaded onto the column at a flow rate of 0.3
846 µL min^{-1} and eluted at a flow rate of 0.25 µL min^{-1} according to the following gradient: 2 to 40%
847 mobile phase B in 150 min and then to 95% in 11 min. Mobile phase B was retained at 95%
848 for 5 min and returned back to 2% a minute after until the end of the run (160 min).
849 Survey scans were recorded at 120,000 resolution (scan range 350-1650 m/z) with an
850 ion target of 5.0e6, and injection time of 20ms. MS2 was performed in the orbitrap at 30,000
851 resolution with a scan range of 200-2000 m/z, maximum injection time of 55ms and AGC
852 target of 3.0E6 ions. We used HCD fragmentation with stepped collision energy of 25.5, 27
853 and 30. We used variable isolation windows throughout the scan range ranging from 10.5 to
854 50.5 m/z. Narrow isolation windows (10.5-18.5 m/z) were applied from 400-800 m/z and then
855 gradually increased to 50.5 m/z until the end of the scan range. The default charge state was
856 set to 3. Data for both survey and MS/MS scans were acquired in profile mode.
857
858 ***Mass spectrometry library search conditions***
859 The DIA-NN software platform (Demichev *et al*, 2020) version 1.9.2. was used to
860 process the DIA raw files and search was conducted against our in house *Saccharomyces*
861 *cerevisiae* complete/reference proteome (original database from Saccharomyces Genome
862 Database for the strain SK1, released in May, 2019). Precursor ion generation was based on
863 the chosen protein database (automatically generated spectral library) with deep-learning
864 based spectra, retention time and IMs prediction. Digestion mode was set to specific with
865 trypsin allowing maximum of two missed cleavages. Carbamidomethylation of cysteine was
866 set as fixed modification. Oxidation of methionine, acetylation of the N-terminus and
867 phosphorylation on serine, threonine and tyrosine were set as variable modifications. The
868 parameters for peptide length range, precursor charge range, precursor m/z range and
869 fragment ion m/z range as well as other software parameters were used with their default

870 values. The precursor FDR was set to 1%. Annotating library proteins were created with
871 information from the FASTA database.
872
873 ***Mass spectrometry data analysis in R***
874 All data analysis was performed using the report.pg_matrix.tsv and
875 report.phosphosites_99.tsv files from DIA-NN version 1.9.2 using R (v 4.2.3) within the
876 RStudio environment.
877 For proteins, the columns corresponding to the measurements of the non-phospho-
878 enriched ("N") samples in the report.pg_matrix.tsv file were analysed. For phospho-sites, the
879 columns corresponding to the measurements of the phospho-enriched ("PE") samples in the
880 report.phosphosites_99.tsv file were analysed. Only phospho-peptides with greater than or
881 equal to 99% localisation confidence for the phospho- modification at the given site residue
882 are included in the measurements in the report.phosphosites_99.tsv file. In DIA-NN, phospho-
883 site abundances can include measurements from multiply-modified peptides, however the
884 vast majority of phospho-sites are quantified from singly phospho-peptides.
885 No imputation was carried out. Due to low coverage, only two out of three replicates
886 of the mitotic DSN1 ("no tag") "N" samples were analysed for protein levels and only two out
887 of three replicates from each of the mitotic DSN1 ("no tag") and mitotic Dsn1-His-Flag ("tag")
888 "PE" samples were analysed for phospho-site abundances. Samples from Dsn1-His-Flag
889 ("tag") IPs and DSN1 ("no tag") IPs were normalised separately. All IP samples of the same
890 type ("tag" or "no tag"), including all replicates and cell cycle stages, were normalised together.
891 For both the protein measurements of the "N" samples and the phospho-site measurements
892 from the "PE" samples, a column median normalisation was carried out; all values in a given
893 sample column were multiplied by a scaling factor consisting of the median intensity of all
894 sample columns divided by the median sample intensity of that individual column. To
895 normalise phospho-site abundances to the protein level, each column-normalised value from
896 the "PE" measurements of the phosphosites_99 file were divided by the corresponding
897 column-normalised protein (from "N") measurement from the pg_matrix table and multiplied
898 by 1000. For example the normalised value of phospho-site Ndc80-T-54 in the PE sample of
899 the phosphosites_99 table was divided by the normalised value of the protein Ndc80 in the
900 corresponding N sample of the pg_matrix and multiplied by 1000.
901 To better analyse differential protein levels between IPs, the protein measurements
902 from the "N" samples were further scaled by the measurement of Dsn1 within each sample.
903 Each normalised protein measurement was divided by the normalised value of Dsn1 within

904 that sample. All protein measurements shown in Figures 4, Supp Fig 5 C-D, and Supp Fig 6-
905 8 are Dsn1-scaled.
906 Protein and phospho-site measurements were further analysed using functions from
907 the Differential Enrichment of Proteins (DEP) R package (Zhang *et al*, 2018). Both protein and
908 phospho-site tables were filtered to include only proteins or sites that were measured in all
909 replicates of at least one condition.
910 Venn diagrams were made using interactivenn.net (Heberle *et al*, 2015). For the GO
911 term enrichment analysis, ranked lists were generated. Proteins or phospho-proteins were
912 ranked by descending fold-change and known kinetochore proteins were excluded. For each
913 stage, comparison with the other stages generated three ranked lists. The top 50 proteins
914 from all three lists were combined together in one list and duplicates were removed. Using
915 these lists, GO term enrichment was carried out using gprofiler2 R package (Kolberg *et al*,
916 2020) with organism="scerevisiae" and otherwise default settings. For the ranked lists in Supp
917 Fig 5 and 9, proteins were ranked by descending fold-change, known kinetochore proteins
918 were excluded, and the top 20 proteins were selected.
919 The stat_pwc() function from the ggpubr R package was used to run statistical tests
920 comparing protein or phospho-site intensities in Figures 4-6 and Supp Fig 7. For boxplots in
921 Figure 4B, Figure 5A, Figure 6C, and Supp Fig 7E-F, a two-sided Wilcoxon test was run and
922 p-values adjusted with the Bonferroni method. For barplots in Figure 5D, a two-sided t-test
923 was run and p-values adjusted with the Bonferroni method. In all figures, a single asterisk (*)
924 indicates a p-value of less than or equal to 0.05, two asterisks (**) a p-value less than or equal
925 to 0.01, and three asterisks (***) p-value of less than or equal to 0.001.
926 The ggseqlogo R package was used to make phospho-site motif logos (Wagih, 2017).
927
928
929
930
931 **Acknowledgements**
932 We are grateful to Sue Biggins, Kevin Hardwick and Patrick Heun for plasmids, to Marina
933 Altamirano De Castro for assistance with plasmid and strain construction, and to Flora Paldi
934 for initial exploratory experiments for induction of metaphase II arrest. We thank Kevin
935 Hardwick and all members of the Marston group for helpful discussions. We gratefully
936 acknowledge the Wellcome Discovery Research Platform for Hidden Cell Biology Proteomics
937 Core for mass spectrometry support. This work was funded through a Wellcome Investigator
938 award to ALM [220780], a Wellcome Multi-User Equipment Grant [218305], core funding for

the Wellcome Centre for Cell Biology [203149] and a Wellcome Discovery Research Platform Award [226791].

Author contributions

Conceptualization – LK and AM; Data curation –LK and CS; Funding Acquisition – AM; Formal Analysis – LK and CS; Investigation – LK; Software – LK; Supervision –AM; Visualization – LK; Writing – original draft – LK; Writing – review and editing – LK and AM with input from all authors

Disclosure and competing interests statement

The authors declare no conflicts of interest.

References

Akiyoshi B, Nelson CR, Ranish JA & Biggins S (2009) Analysis of Ipl1-mediated phosphorylation of the Ndc80 kinetochore protein in Saccharomyces cerevisiae. *Genetics* 183: 1591–1595

Akiyoshi B, Sarangapani KK, Powers AF, Nelson CR, Reichow SL, Arellano-Santoyo H, Gonen T, Ranish JA, Asbury CL & Biggins S (2010) Tension directly stabilizes reconstituted kinetochore-microtubule attachments. *Nature* 468: 576–579

Amin P, Soper Ní Chafraidh S, Leontiou I & Hardwick KG (2018) Regulated reconstitution of spindle checkpoint arrest and silencing through chemically induced dimerisation in vivo. *J Cell Sci* 132: jcs219766

Araki Y, Gombos L, Migueleti SPS, Sivashanmugam L, Antony C & Schiebel E (2010) N-terminal regions of Mps1 kinase determine functional bifurcation. *J Cell Biol* 189: 41–56

Aravamudhan P, Goldfarb AA & Joglekar AP (2015) The kinetochore encodes a mechanical switch to disrupt spindle assembly checkpoint signalling. *Nat Cell Biol* 17: 868–879

Argüello-Miranda O, Zagoriy I, Mengoli V, Rojas J, Jonak K, Oz T, Graf P & Zachariae W (2017) Casein Kinase 1 Coordinates Cohesin Cleavage, Gametogenesis, and Exit from M Phase in Meiosis II. *Dev Cell* 40: 37–52

Barton RE, Massari LF, Robertson D & Marston AL (2022) Eco1-dependent cohesin acetylation anchors chromatin loops and cohesion to define functional meiotic chromosome domains. *Elife* 11: e74447

Benjamin KR, Zhang C, Shokat KM & Herskowitz I (2003) Control of landmark events in meiosis by the CDK Cdc28 and the meiosis-specific kinase Ime2. *Genes & development* 17: 1524–1539

977 Berchowitz LE, Gajadhar AS, van Werven FJ, De Rosa AA, Samoylova ML, Brar GA, Xu Y,
978 Xiao C, Futcher B, Weissman JS, *et al* (2013) A developmentally regulated
979 translational control pathway establishes the meiotic chromosome segregation
980 pattern. *Genes & development* 27: 2147–2163

981 Borek WE, Vincenten N, Duro E, Makrantoni V, Spanos C, Sarangapani KK, de Lima Alves
982 F, Kelly DA, Asbury CL, Rappsilber J, *et al* (2021) The Proteomic Landscape of
983 Centromeric Chromatin Reveals an Essential Role for the Ctf19CCAN Complex in
984 Meiotic Kinetochore Assembly. *Curr Biol* 31: 283-296.e7

985 Buonomo SBC, Rabitsch KP, Fuchs J, Gruber S, Sullivan M, Uhlmann F, Petronczki M, Tóth
986 A & Nasmyth K (2003) Division of the nucleolus and its release of CDC14 during
987 anaphase of meiosis I depends on separase, SPO12, and SLK19. *Developmental cell*
988 4: 727–739

989 Carlile TM & Amon A (2008) Meiosis I is established through division-specific translational
990 control of a cyclin. *Cell* 133: 280–291

991 Chen C, Whitney IP, Banerjee A, Sacristan C, Sekhri P, Kern DM, Fontan A, Kops GJPL,
992 Tyson JJ, Cheeseman IM, *et al* (2019) Ectopic Activation of the Spindle Assembly
993 Checkpoint Signaling Cascade Reveals Its Biochemical Design. *Curr Biol* 29: 104-
994 119.e10

995 Chen J, Liao A, Powers EN, Liao H, Kohlstaedt LA, Evans R, Holly RM, Kim JK, Jovanovic M
996 & Ünal E (2020) Aurora B-dependent Ndc80 degradation regulates kinetochore
997 composition in meiosis. *Genes Dev* 34: 209–225

998 Chia M & van Werven FJ (2016) Temporal Expression of a Master Regulator Drives
999 Synchronous Sporulation in Budding Yeast. *G3 (Bethesda, Md)* 6: 3553–3560

1000 Clyne RK, Katis VL, Jessop L, Benjamin KR, Herskowitz I, Lichten M & Nasmyth K (2003)
1001 Polo-like kinase Cdc5 promotes chiasmata formation and cosegregation of sister
1002 centromeres at meiosis I. *Nat Cell Biol* 5: 480–485

1003 Demichev V, Messner CB, Vernardis SI, Lilley KS & Ralser M (2020) DIA-NN: neural networks
1004 and interference correction enable deep proteome coverage in high throughput. *Nat*
1005 *Methods* 17: 41–44

1006 Duro E & Marston AL (2015) From equator to pole: splitting chromosomes in mitosis and
1007 meiosis. *Genes Dev* 29: 109–122

1008 Fernius J & Marston AL (2009) Establishment of cohesion at the pericentromere by the Ctf19
1009 kinetochore subcomplex and the replication fork-associated factor, Csm3. *PLoS Genet*
1010 5: e1000629

1011 Ghodgaonkar-Steger M, Potocnjak M, Zimniak T, Fischböck-Halwachs J, Solis-Mezarino V,
1012 Singh S, Speljko T, Hagemann G, Drexler DJ, Witte G, *et al* (2020) C-Terminal Motifs
1013 of the MTW1 Complex Cooperatively Stabilize Outer Kinetochore Assembly in Budding
1014 Yeast. *Cell Rep* 32: 108190

1015 Gruhn JR & Hoffmann ER (2022) Errors of the Egg: The Establishment and Progression of
1016 Human Aneuploidy Research in the Maternal Germline. *Annu Rev Genet* 56: 369–390

1017 Gui L & Homer H (2012) Spindle assembly checkpoint signalling is uncoupled from
1018 chromosomal position in mouse oocytes. *Development* 139: 1941–1946

1019 Havens KA, Gardner MK, Kamieniecki RJ, Dresser ME & Dawson DS (2010) Slk19p of
1020 Saccharomyces cerevisiae regulates anaphase spindle dynamics through two
1021 independent mechanisms. *Genetics* 186: 1247–1260

1022 Hayashi A, Asakawa H, Haraguchi T & Hiraoka Y (2006) Reconstruction of the kinetochore
1023 during meiosis in fission yeast Schizosaccharomyces pombe. *Molecular biology of the*
1024 *cell* 17: 5173–5184

1025 Heberle H, Meirelles GV, da Silva FR, Telles GP & Minghim R (2015) InteractiVenn: a web-
1026 based tool for the analysis of sets through Venn diagrams. *BMC Bioinformatics* 16:
1027 169

1028 Hochwagen A, Wrobel G, Cartron M, Demougin P, Niederhauser-Wiederkehr C, Boselli MG,
1029 Primig M & Amon A (2005) Novel response to microtubule perturbation in meiosis. *Mol*
1030 *Cell Biol* 25: 4767–4781

1031 Holt LJ, Tuch BB, Villén J, Johnson AD, Gygi SP & Morgan DO (2009) Global analysis of Cdk1
1032 substrate phosphorylation sites provides insights into evolution. *Science* 325: 1682

1033 Iwabuchi M, Ohsumi K, Yamamoto TM, Sawada W & Kishimoto T (2000) Residual Cdc2
1034 activity remaining at meiosis I exit is essential for meiotic M-M transition in Xenopus
1035 oocyte extracts. *EMBO J* 19: 4513–4523

1036 Koch LB, Spanos C, Kelly V, Ly T & Marston AL (2024) Rewiring of the phosphoproteome
1037 executes two meiotic divisions in budding yeast. *EMBO J* 43: 1351–1383

1038 Kolano A, Brunet S, Silk AD, Cleveland DW & Verlhac M-H (2012) Error-prone mammalian
1039 female meiosis from silencing the spindle assembly checkpoint without normal
1040 interkinetochore tension. *Proceedings of the National Academy of Sciences* 109:
1041 E1858–E1867

1042 Kolberg L, Raudvere U, Kuzmin I, Vilo J & Peterson H (2020) gprofiler2 -- an R package for
1043 gene list functional enrichment analysis and namespace conversion toolset g:Profiler.
1044 *F1000Res* 9: ELIXIR-709

1045 Kouznetsova A, Kitajima TS, Brismar H & Höög C (2019) Post-metaphase correction of
1046 aberrant kinetochore-microtubule attachments in mammalian eggs. *EMBO Rep* 20:
1047 e47905

1048 Lane SIR, Yun Y & Jones KT (2012) Timing of anaphase-promoting complex activation in
1049 mouse oocytes is predicted by microtubule-kinetochore attachment but not by bivalent
1050 alignment or tension. *Development* 139: 1947–1955

1051 Lee BH & Amon A (2003) Role of Polo-like kinase CDC5 in programming meiosis I
1052 chromosome segregation. *Science (New York, NY)* 300: 482–486

1053 Leontiou I, London N, May KM, Ma Y, Grzesiak L, Medina-Pritchard B, Amin P, Jeyaprakash
1054 AA, Biggins S & Hardwick KG (2019) The Bub1-TPR Domain Interacts Directly with
1055 Mad3 to Generate Robust Spindle Checkpoint Arrest. *Curr Biol* 29: 2407-2414.e7

1056 Liang F-S, Ho WQ & Crabtree GR (2011) Engineering the ABA plant stress pathway for
1057 regulation of induced proximity. *Sci Signal* 4: rs2

1058 Liu D, Vleugel M, Backer CB, Hori T, Fukagawa T, Cheeseman IM & Lampson MA (2010)
1059 Regulated targeting of protein phosphatase 1 to the outer kinetochore by KNL1
1060 opposes Aurora B kinase. *J Cell Biol* 188: 809–820

1061 Lo HC, Wan L, Rosebrock A, Futcher B & Hollingsworth NM (2008) Cdc7-Dbf4 regulates
1062 NDT80 transcription as well as reductional segregation during budding yeast meiosis.
1063 *Molecular biology of the cell* 19: 4956–4967

1064 MacKenzie A, Vicory V & Lacefield S (2023) Meiotic cells escape prolonged spindle
1065 checkpoint activity through kinetochore silencing and slippage. *PLoS Genet* 19:
1066 e1010707

1067 Marston AL, Lee BH & Amon A (2003) The Cdc14 phosphatase and the FEAR network control
1068 meiotic spindle disassembly and chromosome segregation. *Dev Cell* 4: 711–726

1069 Maskell DP, Hu X-W & Singleton MR (2010) Molecular architecture and assembly of the yeast
1070 kinetochore MIND complex. *J Cell Biol* 190: 823–834

1071 Matos J, Lipp JJ, Bogdanova A, Guillot S, Okaz E, Junqueira M, Shevchenko A & Zachariae
1072 W (2008) Dbf4-dependent CDC7 kinase links DNA replication to the segregation of
1073 homologous chromosomes in meiosis I. *Cell* 135: 662–678

1074 McAinsh AD & Kops GJPL (2023) Principles and dynamics of spindle assembly checkpoint
1075 signalling. *Nat Rev Mol Cell Biol* 24: 543–559

1076 Mehta GD, Agarwal M & Ghosh SK (2014) Functional characterization of kinetochore protein,
1077 Ctf19 in meiosis I: An implication of differential impact of Ctf19 on the assembly of
1078 mitotic and meiotic kinetochores in Saccharomyces cerevisiae. *Molecular Microbiology*
1079 91: 1179–1199

1080 Mengoli V, Jonak K, Lyzak O, Lamb M, Lister LM, Lodge C, Rojas J, Zagoriy I, Herbert M &
1081 Zachariae W (2021) Deprotection of centromeric cohesin at meiosis II requires APC/C
1082 activity but not kinetochore tension. *EMBO J* 40: e106812

1083 Meyer RE, Chuong HH, Hild M, Hansen CL, Kinter M & Dawson DS (2015) Ipl1/Aurora-B is
1084 necessary for kinetochore restructuring in meiosis I in Saccharomyces cerevisiae.
1085 *Molecular biology of the cell* 26: 2986–3000

1086 Miller MP, Ünal E, Brar GA & Amon A (2012) Meiosis I chromosome segregation is established
1087 through regulation of microtubule–kinetochore interactions. *eLife* 1: e00117

1088 Miyazono K-I, Miyakawa T, Sawano Y, Kubota K, Kang H-J, Asano A, Miyauchi Y, Takahashi
1089 M, Zhi Y, Fujita Y, *et al* (2009) Structural basis of abscisic acid signalling. *Nature* 462:
1090 609–614

1091 Nagaoka SI, Hodges CA, Albertini DF & Hunt PA (2011) Oocyte-Specific Differences in Cell-
1092 Cycle Control Create an Innate Susceptibility to Meiotic Errors. *Current Biology* 21:
1093 651–657

1094 Palframan WJ, Meehl JB, Jaspersen SL, Winey M & Murray AW (2006) Anaphase inactivation
1095 of the spindle checkpoint. *Science (New York, NY)* 313: 680–684

1096 Peshkin L, Daldello EM, Itallie EV, Sonnett M, Kreuzer J, Haas W, Kirschner MW & Jessus C
1097 (2025) Decoding protein phosphorylation during oocyte meiotic divisions using
1098 phosphoproteomics. *eLife* 13

1099 Peters J-M (2006) The anaphase promoting complex/cyclosome: a machine designed to
1100 destroy. *Nat Rev Mol Cell Biol* 7: 644–656

1101 Petronczki M, Matos J, Mori S, Gregan J, Bogdanova A, Schwickart M, Mechtler K, Shirahige
1102 K, Zachariae W & Nasmyth K (2006) Monopolar attachment of sister kinetochores at
1103 meiosis I requires casein kinase 1. *Cell* 126: 1049–1064

1104 Petrovic A, Mosalaganti S, Keller J, Mattiuzzo M, Overlack K, Krenn V, De Antoni A,
1105 Wohlgemuth S, Cecatiello V, Pasqualato S, *et al* (2014) Modular assembly of RWD
1106 domains on the Mis12 complex underlies outer kinetochore organization. *Mol Cell* 53:
1107 591–605

1108 Pinsky BA, Kung C, Shokat KM & Biggins S (2006) The Ipl1-Aurora protein kinase activates
1109 the spindle checkpoint by creating unattached kinetochores. *Nat Cell Biol* 8: 78–83

1110 Plowman R, Singh N, Tromer EC, Payan A, Duro E, Spanos C, Rappsilber J, Snel B, Kops
1111 GJPL, Corbett KD, *et al* (2019) The molecular basis of monopolin recruitment to the
1112 kinetochore. *Chromosoma* 128: 331–354

1113 Ptacek J, Devgan G, Michaud G, Zhu H, Zhu X, Fasolo J, Guo H, Jona G, Breitkreutz A, Sopko
1114 R, *et al* (2005) Global analysis of protein phosphorylation in yeast. *Nature* 438: 679–
1115 684

1116 Rappsilber J, Mann M & Ishihama Y (2007) Protocol for micro-purification, enrichment, pre-
1117 fractionation and storage of peptides for proteomics using StageTips. *Nat Protoc* 2:
1118 1896–1906

1119 Rosenberg JS, Cross FR & Funabiki H (2011) KNL1/Spc105 Recruits PP1 to Silence the
1120 Spindle Assembly Checkpoint. *Curr Biol* 21: 942–947

1121 Roy B, Sim J, Han SJY & Joglekar AP (2022) Kre28-Spc105 interaction is essential for Spc105
1122 loading at the kinetochore. *Open Biol* 12: 210274

1123 Roy B, Verma V, Sim J, Fontan A & Joglekar AP (2019) Delineating the contribution of
1124 Spc105-bound PP1 to spindle checkpoint silencing and kinetochore microtubule
1125 attachment regulation. *J Cell Biol* 218: 3926–3942

1126 Sarangapani KK, Akiyoshi B, Duggan NM, Biggins S & Asbury CL (2013) Phosphoregulation
1127 promotes release of kinetochores from dynamic microtubules via multiple
1128 mechanisms. *Proc Natl Acad Sci USA* 110: 7282–7287

1129 Sarangapani KK, Duro E, Deng Y, Alves F de L, Ye Q, Opoku KN, Ceto S, Rappsilber J,
1130 Corbett KD, Biggins S, *et al* (2014) Sister kinetochores are mechanically fused during
1131 meiosis I in yeast. *Science* 346: 248–251

1132 Sarkar S, Shenoy RT, Dalgaard JZ, Newnham L, Hoffmann E, Millar JBA & Arumugam P
1133 (2013) Monopolin subunit Csm1 associates with MIND complex to establish monopolar
1134 attachment of sister kinetochores at meiosis I. *PLoS Genet* 9: e1003610

1135 Sebestova J, Danylevska A, Novakova L, Kubelka M & Anger M (2012) Lack of response to
1136 unaligned chromosomes in mammalian female gametes. *Cell Cycle* 11: 3011–3018

1137 Stegmeier F, Visintin R & Amon A (2002) Separase, polo kinase, the kinetochore protein
1138 Slk19, and Spo12 function in a network that controls Cdc14 localization during early
1139 anaphase. *Cell* 108: 207–220

1140 Sullivan M, Lehane C & Uhlmann F (2001) Orchestrating anaphase and mitotic exit: separase
1141 cleavage and localization of Slk19. *Nat Cell Biol* 3: 771–777

1142 Wagih O (2017) ggseqlogo: a versatile R package for drawing sequence logos. *Bioinformatics*
1143 33: 3645–3647

1144 Wettstein R, Hugener J, Gillet L, Hernández-Armenta Y, Henggeler A, Xu J, van Gerwen J,
1145 Wollweber F, Arter M, Aebersold R, *et al* (2024) Waves of regulated protein expression
1146 and phosphorylation rewire the proteome to drive gametogenesis in budding yeast.
1147 *Dev Cell* 59: 1764-1782.e8

1148 Wiśniewski JR, Zougman A, Nagaraj N & Mann M (2009) Universal sample preparation
1149 method for proteome analysis. *Nat Methods* 6: 359–362

1150 Zhang X, Smits AH, van Tilburg GB, Ovaa H, Huber W & Vermeulen M (2018) Proteome-wide
1151 identification of ubiquitin interactions using UbIA-MS. *Nat Protoc* 13: 530–550

1152

1153

1154

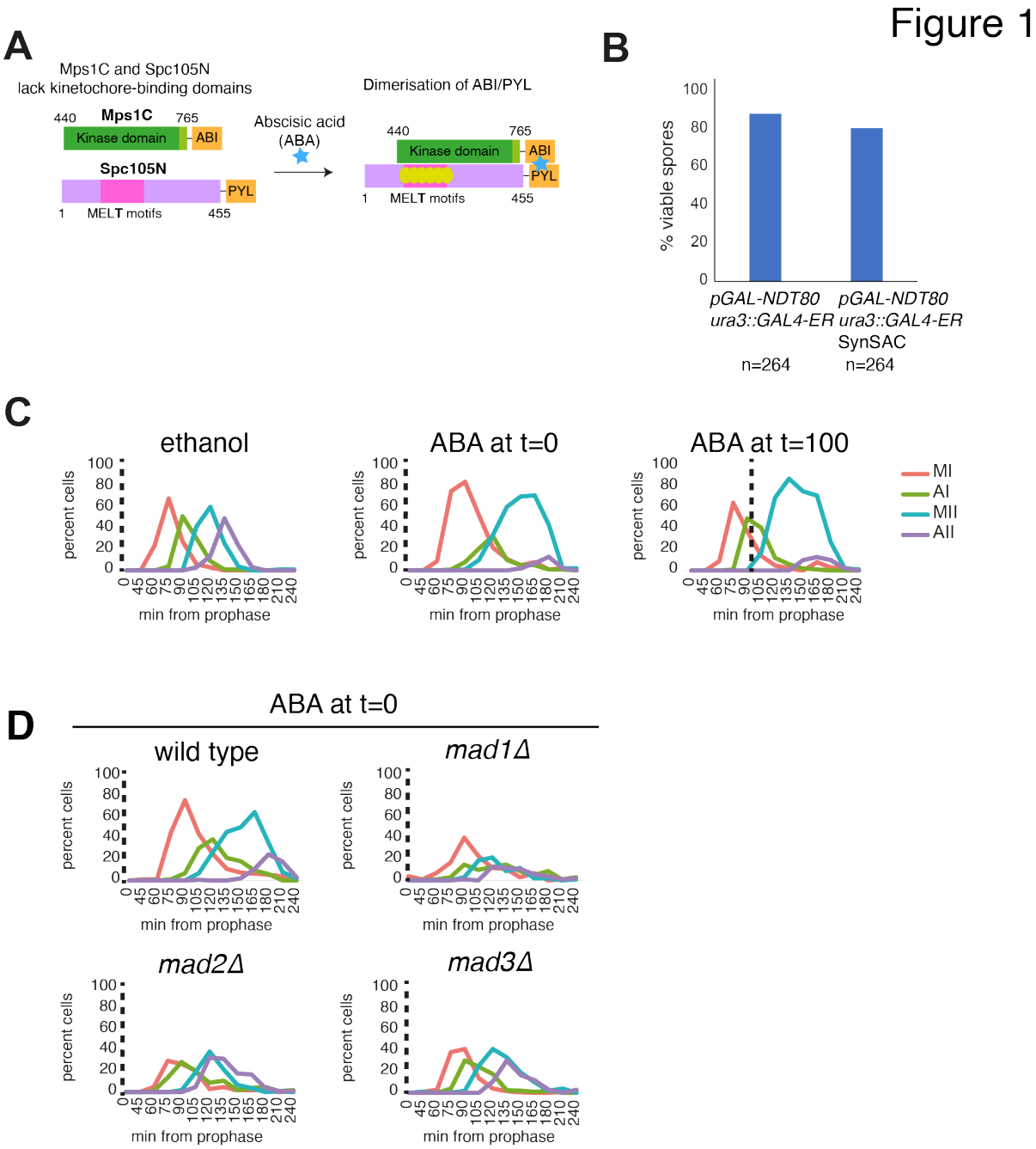

Figure 1 Construction of a meiotic SynSAC activation system

(A) Diagram of synthetic SAC dimerization system. (B) Spore viability of wild type (AM11189) and SynSAC dimer (AM30783) yeast strains (C) Meiosis spindle immunofluorescence timecourse of SynSAC dimer yeast strain (AM30783) under control (ethanol, left), meiosis I dimerizing (250μM ABA at release), or meiosis II dimerizing (250μM ABA at 100 minutes) conditions. (D) Meiosis spindle immunofluorescence timecourse in wild-type SynSAC (AM30783), SynSAC *mad1Δ* (AM33558), SynSAC *mad2Δ* (AM33559), and SynSAC *mad3Δ* (AM30784) strains. Vertical dotted line indicates time of ABA addition. 250μM abscisic acid

1164 (ABA) was added to each culture at 0 minutes upon addition of β-estradiol (prophase release).

1165 MI = metaphase I; AI = anaphase I; MII = metaphase II; AII = anaphase II.

1166

1167

Figure 2

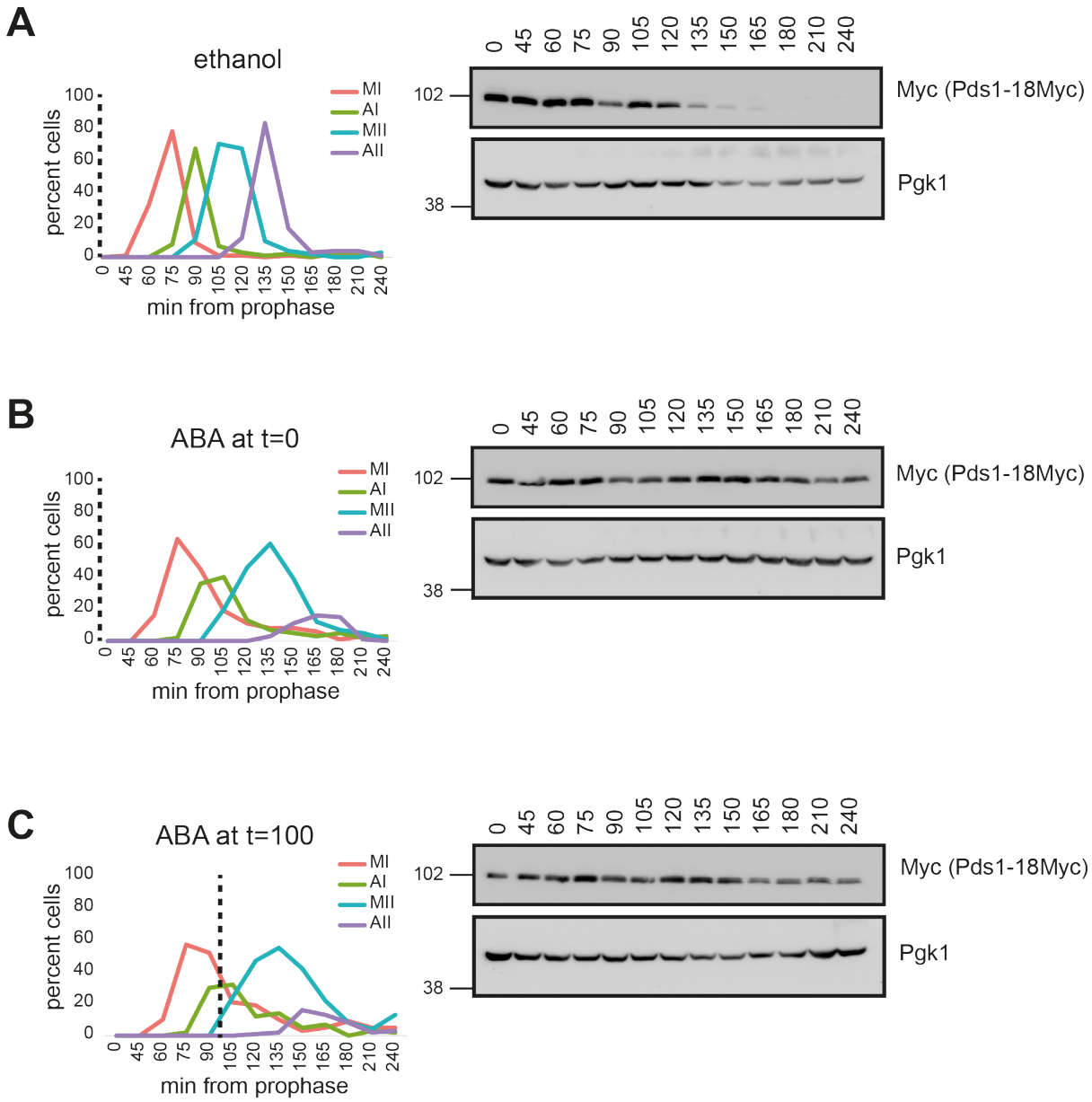

Figure 2 Meiotic SynSAC delays degradation of Pds1^{securin}

(A-C) Meiosis timecourse with spindle immunofluorescence (left) and western blotting to visualize Pds1-Myc and Pgk1 loading control (right). (A) Control timecourse with ethanol added at prophase release (vertical dotted line). (B) Meiosis I SynSAC delay timecourse with 250μM ABA added at prophase release (vertical dotted line). (C) Meiosis II SynSAC delay meiosis timecourse with 250μm ABA added at 100 minutes after prophase release (vertical dotted line). Strain used in A-C was AM34398. MI = metaphase I; AI = anaphase I; MII = metaphase II; AII = anaphase II.

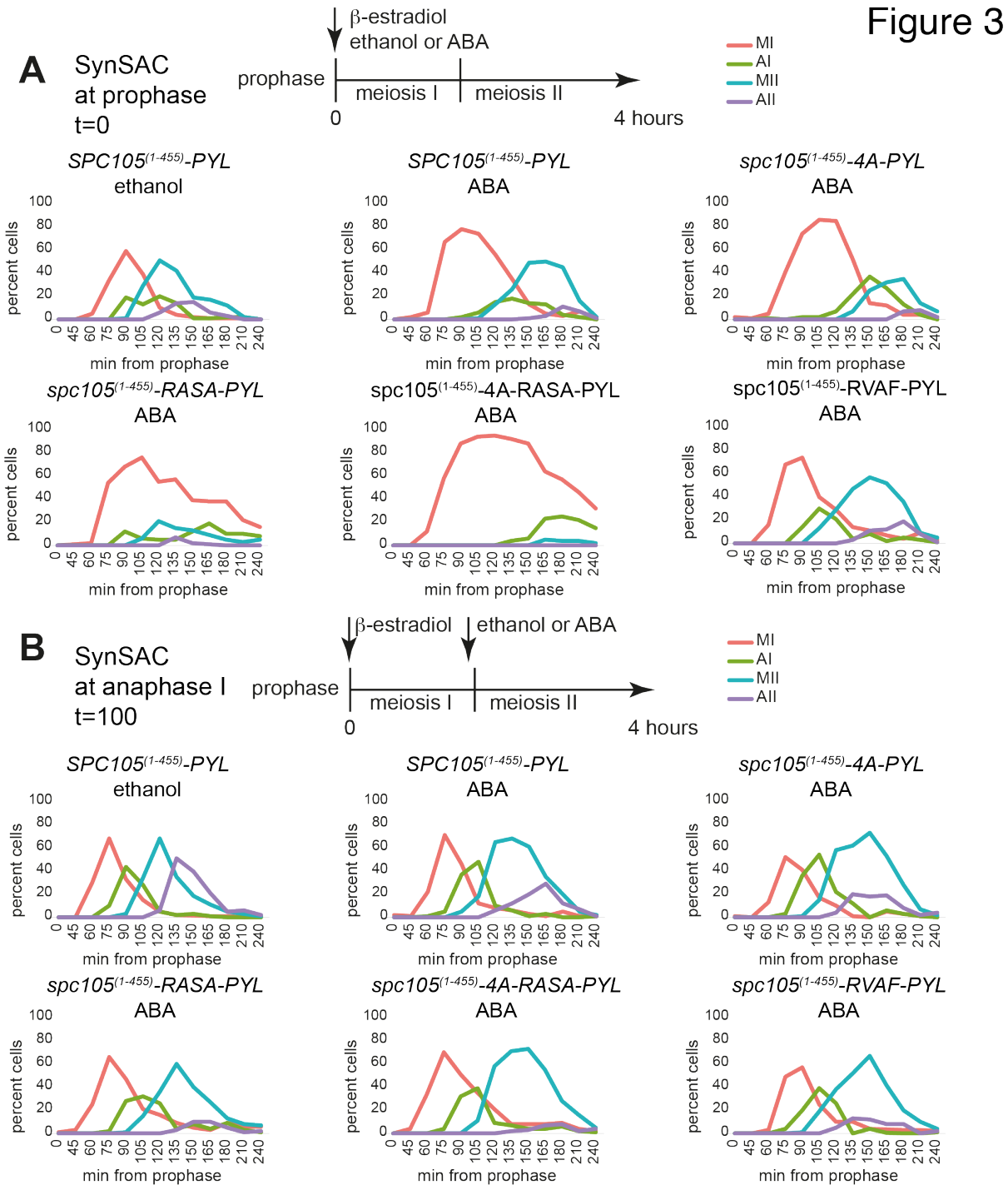

Figure 3 PP1 binding restrains SynSAC delay duration in meiotic metaphase

(A-B) Meiosis I (A) and meiosis II (B) SynSAC spindle immunofluorescence timecourses in wild-type vs PP1 binding site mutant SynSAC strains. Top: Schematic indicating drug addition timing. Middle row: Control wild-type (AM30783), SynSAC wild-type (AM30783), SynSAC *spc105-4A* (AM34201). Bottom row: SynSAC *spc105-RASA* (AM34203), SynSAC *spc105-4A-RASA* (AM34202), SynSAC *spc105-RVAF* (AM34487).

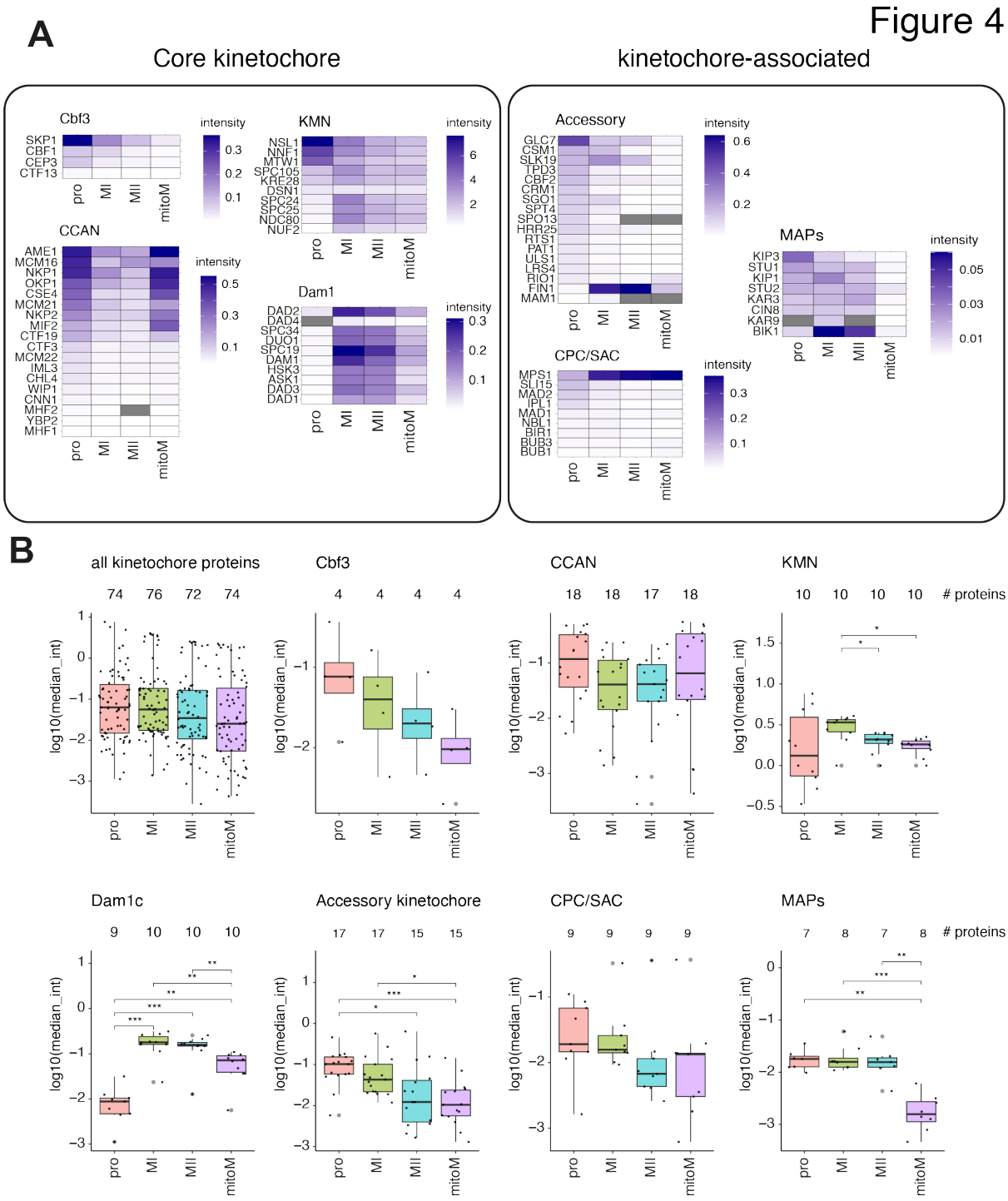

Figure 4 Kinetochore protein dynamics in meiotic prophase, metaphase I, metaphase II, and mitotic metaphase

(A and B) Knetochores purified by Dsn1-6His-3Flag immunoprecipitation were analysed from cells arrested at the indicated stages using the SynSAC system by mass spectrometry. Strain used was AM33675. (A) Heatmap of individual protein levels of core kinetochore proteins (left). Heatmap of individual protein levels of transiently associated kinetochore proteins at each stage (right). (B) Boxplots of groups of kinetochore proteins at each stage. Dots indicate

individual proteins and the numbers above each plot indicate the number of proteins included in each group at that stage. P-values from Wilcoxon two-sided test are shown.

Figure 5

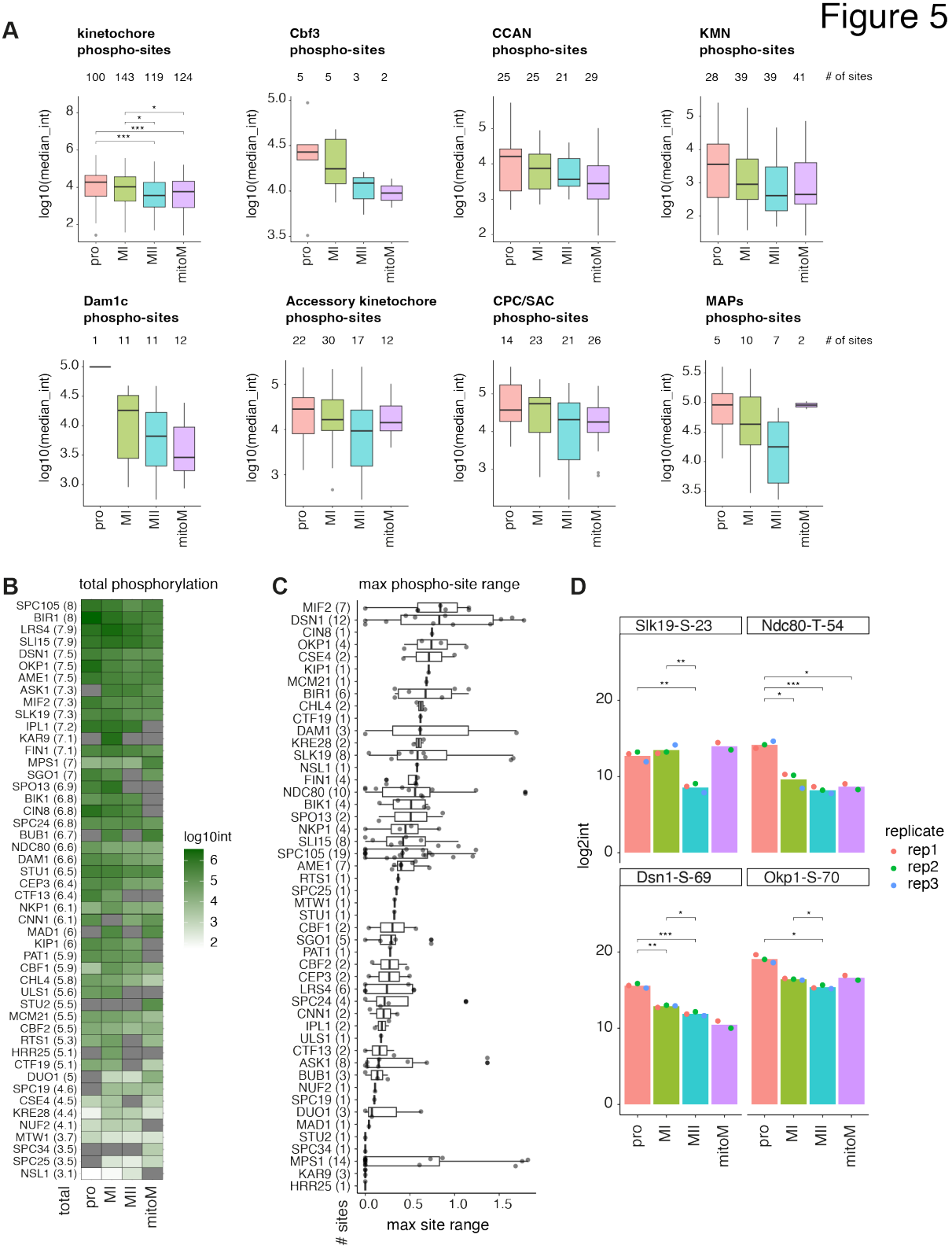

Figure 5 Reduced kinetochore protein phosphorylation in metaphase II

(A-D) Phosphorylation analysis of kinetochores purified as in Figure 4 and subjected to phospho-enrichment prior to mass spectrometry. (A)Boxplots of groups of kinetochore protein phosphorylation sites at each stage. Numbers above each plot indicate the number of phospho-sites included in the group at each stage. P-values from two-sided Wilcoxon test are

1204 shown for all kinetochore phospho-sites (upper left). No other comparisons were significantly
1205 different by Wilcoxon test in any other group/stage. (B) Heatmap of total sum of phospho-site
1206 abundance for each kinetochore protein at each stage. Phospho-proteins are ranked, with
1207 proteins with the highest sum of phospho-site abundances, for all 4 stages together, at the
1208 top. Numbers within parentheses next to protein name indicate the sum of phospho-site
1209 abundances for all 4 stages. (C) Boxplots of maximum phospho-site range across the 4 stages
1210 for each kinetochore protein. Phospho-proteins are ranked so that proteins with the highest
1211 median phospho-site dynamic range across stages are at the top. Numbers in parentheses
1212 indicate the number of phospho-sites considered to calculate maximum phospho-site range.
1213 (D) Barplots of individual phospho-site abundances for the indicated sites at each of the 4
1214 stages. Dots indicate the abundance in individual replicates.
1215
1216

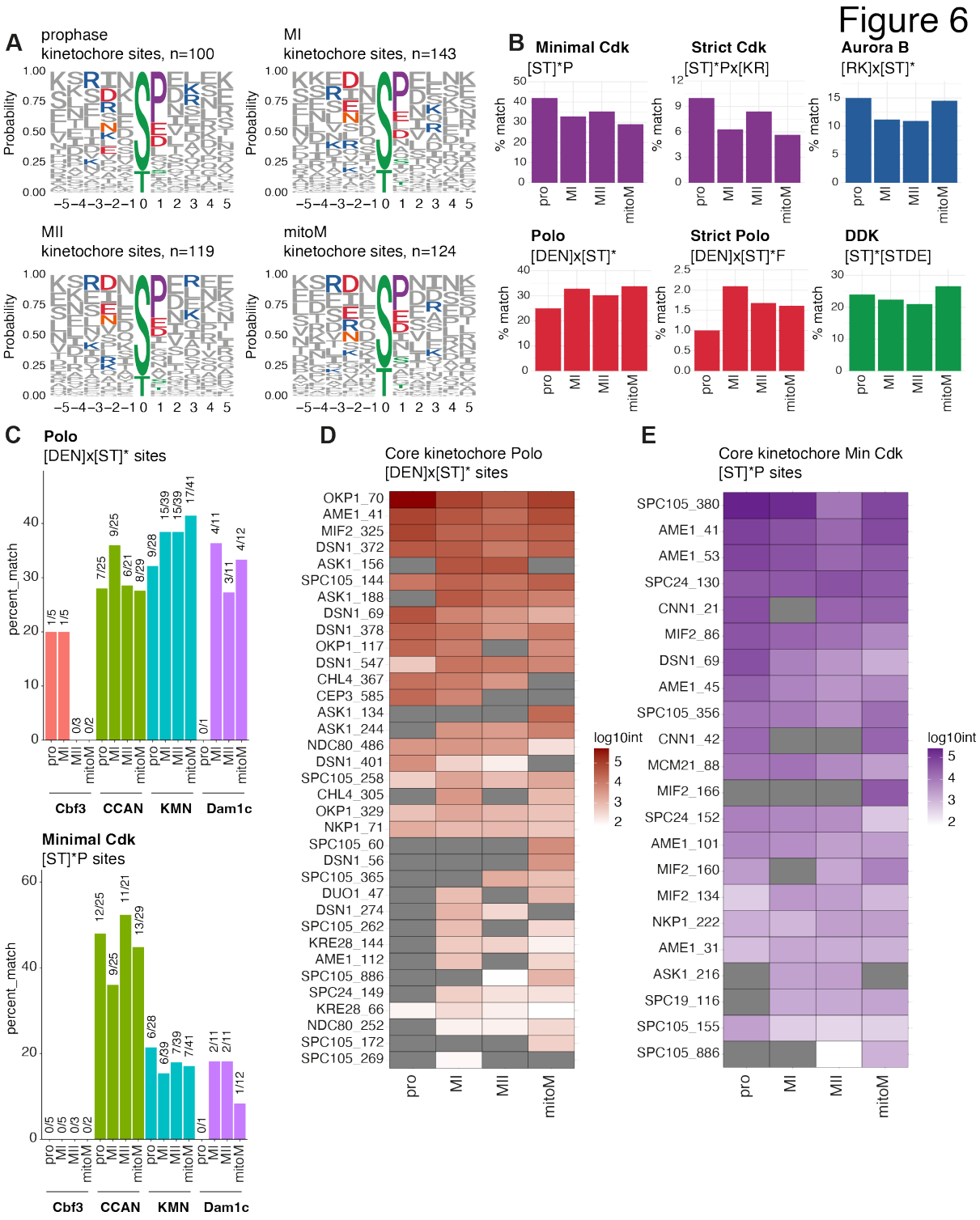

Figure 6 Kinetochore phospho-site motifs do not vary significantly by stage

(A-D) Features of kinetochore phosphorylation after phospho-analysis of kinetochore purifications in Figure 5. (A) Motif logos of amino acids surrounding kinetochore protein phospho-sites at each stage. (B) Barplots of the percent of phospho-sites which match indicated kinase consensus motifs at each stage. (C) Barplots of the percent of phospho-sites which match the Polo kinase consensus motif (top) or minimal Cdk consensus motif (bottom),

1224 sorted by kinetochore sub-complex and cell cycle stage. (D) Heatmap showing the abundance
1225 of individual kinetochore phospho-sites matching the minimal Polo kinase consensus. (E)
1226 Heatmap showing the abundance of individual kinetochore phospho-sites matching the
1227 minimal Cdk kinase consensus.